WIDE-BANDWIDTH TIME OF FLIGHT SPECTROSCOPY OF TURBID MEDIA

Master's Thesis

By

Arman Ahamed Subash

Lund University

ABSTRACT

Wide bandwidth time-of-flight spectrometer (TOFS) developed in the Group of Biophotonics, Lund University, is a unique tool which is capable to deliver continues absorption/scattering spectra of turbid samples in a singularly broad wavelength range from 600nm up to 1400nm. The main focus of this thesis work is to calibrate and optimize the performance of the instrumental setup of this system for biomedical & pharmaceutical applications ensuring the capability to produce results with high accuracy and repeatability. In this spectroscopy, the precision of the measurements heavily relies on precise timing calibration of the system and accurate determination of the instrumental response function (IRF). A new double path optical scheme was implemented in this system, for adding Time Reference Pulse to circumvent the uncertainty occurred in the results due to apparent source and detector temporal drifts and finite resolution of the TCSPC detection. This technique brings success to maintain high measurement precision (uncertainty less than 1 %). The accurate calibration of the system was performed by measuring the reduced scattering coefficient (μ'_s) of pure Intralipid-20% and absorption coefficient (μ_a) of Indian ink solution. For performance assessment of the system, different types of experiments including verification of repeatability, verification of linearity in performance, verification of the consistency of the experimental data along with theoretical model were executed preparing different type of solid and liquid phantoms. All these experiments showed acceptable results. New type of epoxy phantom was developed with BG36 filter crashed powder and TiO_2 for providing remarkably different absorptions at different wavelengths which is very effective for calibration of the system. Limited resolution effects of the system for finite source resolution and dispersion in probe pulse were also explored using this phantom. Time-of-flight spectroscopy (TOFS) was also implemented in order to measure Active Pharmaceutical Ingredient (API) of the pharmaceutical tablets. Continuous scattering and absorption spectra of real tablets were acquired at NIR region with the resolution/step of 4 nm. The estimated API concentrations by PLS regression are within 10% of the reference values.

POPULAR SCIENCE

There are many everyday objects like milk, snow, paper (and importantly biological tissues, pharmaceutical tablets) where propagation of light is highly affected by scattering. These are known as turbid or highly scattering materials. Using conventional absorption spectroscopy, absorption measurement of such materials is rigorously affected by the scattering and it is not possible to decouple absorption and scattering properties. For evaluating absorption/scattering properties of such turbid samples in a broad wavelength range from 600nm to 1400nm, a system called wide bandwidth time-of-flight spectrometer (TOFS) was built in Atomic Physics Division at Lund University. Estimated scattering and absorption properties enable the analysis of their chemical composition and structural properties. The focus of my thesis work is to develop the setup of Photon Time-of-Flight Spectrometer for biomedical & pharmaceutical applications. Main idea of this spectroscopic technique is to inject a very short pulse of light through a medium and observe the broadening of the pulse due to multiple scattering events. In this spectroscopy, the accurate measurements of the scattering and absorption properties heavily depend on the accurate measurement of the broadened pulse in time domain. The incompetence of the light source and detector, used in this system, for generating and detecting light pulse precisely on time scale lead to poor precision in results. To circumvent this problem, a very new idea was implemented by for getting the correct position of the broadened light pulse in time domain and it brings us the opportunity to get the results with precision ten times higher than before and with very high accuracy. For performance assessment of the system, different types of experimental tests were executed preparing different types of solid and liquid phantoms. Phantom is such a simulating object which has similar optical properties of any turbid material. Solid phantoms were prepared with epoxy, resin, hardener, TiO2 powder (scatterer) and toner (absorber), while liquid phantoms were prepared with water, Intralipid (scatterer) and Indian ink (absorber). All these experiments showed acceptable results.

After achieving very good stability, this system was implemented for measuring the drug concentration (API) of the pharmaceutical tablets. It is a very important issue for proper treatment of any disease as well as for consumers' rights. Pharmaceuticals tablets are highly scattering. With conventional absorption spectroscopy, the tablets' abortion measurements are severely affected by the scattering which also affect the determination of drug concentration. For pilot experiment, total 54 tablets were prepared with six different concentration of drug and with three different level scattering. As a first step, continuous scattering and absorption spectra of four real tablets were obtained separately at near infrared region with the resolution/step of 4nm. Then absorption and scattering coefficient of 54 tablets were measured at eight different wavelengths. Then, a statistical method called partial least square regression was made with the absorption values in order to estimate the drug concentration.

ABBREVIATIONS

VIS	Visible
NIR	Near Infrared
PTOFS	Photon Time-of-Flight Spectroscopy
TCSPC	Time-correlated Single Photon Counting
API	Active Pharmaceutical Ingredient
DA	Diffusion Approximation
DE	Diffusion Equation
IRF	Instrumental Response Function
WMC	White Monte Carlo
APD	Avalanche Photo Diode
PMT	Photo Multiplier Tube

CONTENTS

Chapter 1

1 Introduction:

The spectroscopy of turbid (highly scattering) materials in VIS and NIR regions is very important in the field of bio-photonics, biomedical and industrial applications. Conventional absorption spectroscopy, based on the quantitative loss of intensity due to transmission through samples, is very efficient for measuring the absorption of the sample where the optical path length is known. However, it is limited for turbid material due to multiple scattering events. This multiple scattering nature of the medium demands the developments of sensitive instrumentation for photon detection and sophisticated physical model for propagation of photon into the medium for extracting correct optical properties. Wide bandwidth Photon Time-of-Flight Spectroscopy (PTOFS) is such an approach which enables the determination of the optical properties separately where light scattering is stronger than absorption. In this technique, the detected signal is evaluated not only considering the absorption effect but also considering the unknown path length distribution and the geometrically determined losses of light due to scattering [1].

Photon Time-of-Flight Spectroscopy is designed for analysis of highly scattering materials. It enables the analysis of chemical composition and structural properties of any turbid material like biological tissues, pharmaceutical tablets, foods, agricultural products and so on. It can be applied for non-invasive biomedical diagnostics and precise treatment monitoring, quality control of food and agricultural products, determination of API (Active Pharmaceutical Ingredient) in pharmaceutical tablets and so on.

The aim of this thesis work was to calibrate and optimize the performance of the instrumental setup of Ultra-wide bandwidth Photon Time-of-Flight Spectroscopy (PTOFS) for biomedical & pharmaceutical applications. In this spectroscopy, the precision of the measurements heavily relies upon precise timing calibration of the system. The uncertainty in timing calibration affects the results and leads to poor precision in measurements. To

circumvent this problem, double path optical scheme was introduced. Then, performance of the system was assessed by performing different types of experiments preparing different type of solid and liquid phantoms. New type of epoxy phantom was also developed for calibration of the system and limited resolution effects of the system were observed when its optical properties were measured. Optical properties of real pharmaceutical tables were evaluated in order to measure their Active Pharmaceutical Ingredient (API) concentrations.

Chapter 2

2. Optical Properties and Spectroscopy:

2.1 Optical Properties:

In order to determine the chemical composition, physical or structural properties of the material by spectroscopy, it is very important to understand the interaction of incident light with media. When any turbid medium like tissue or pharmaceuticals tablet, is irradiated by light, some of the light will be reflected off the surface, while the rest enters the medium. Inside the medium, light can be absorbed or scattered by the particles.

The amount of absorption and scattering depend on the concentration and size of the particles. Absorption increases with increasing the concentration of the absorbing particles while scattering increases with decreasing the particle size and increasing the concentration of scattering particles. Scattering is mainly of two kinds e.g. Elastic and Inelastic scattering. Elastic scattering occurred when there is no change in photon energy such as in Rayleigh and Mie scattering. When particle size is much smaller than the incident wavelength, Rayleigh scattering is occurred and Mie scattering is occurred when the particle size becomes comparable to wavelength.

The amount of absorption and scattering is defined by the absorption coefficient μ_a and scattering coefficient μ_s or reduced scattering coefficient μ'_s respectively. The absorption coefficient μ_a gives the probability for a photon to be absorbed per unit path length. It also determines how far into a material, light of a particular wavelength can penetrate before it is absorbed. The scattering coefficient μ_s gives the probability for a photon to be scattered per unit path length or the average number of scatterings per unit path length. For high scattering material, like tissue, it is required to define scattering by reduced scattering coefficient $\mu'_s = (1-g)\ \mu_s$, where, g is the anisotropy coefficient and used to describe the angular distribution of the light scattering. The scattering and absorption properties are strongly wavelength dependent and the stronger the absorption, the smaller the penetration depth of that particular wavelength.

2.2 Conventional Absorption Spectroscopy & PTOF Spectroscopy:

The fundamental assumption for conventional absorption spectroscopy is that the main loss mechanism is absorption, and here absorption is measured by counting the net loss of intensity after passing through the sample and following Beer-Lambert law of absorption. According to Beer-Lambert law:

$$I(L) = I_0 \exp(-\mu_a L)$$

Where I_0 initial photon intensity of light before passing through the sample, L is path length, $I(L)$ is intensity of light after passing through the sample and μ_a is the absorption coefficient of the medium.

For non-scattering medium it is easy to calculate path length. However, for scattering medium it is not feasible due to multiple scattering events. Applying conventional absorption spectroscopy in scattering medium, only extinction spectra can be obtained which is the interplay of absorption and scattering.

On the other hand, in PTOF Spectroscopy, it is possible to measure the scattering and absorption of scattering material separately. In this technique intensity is only important to maintain the signal to noise ratio. Main idea is to observe the broadening of the injected short laser pulse through the medium. A very short laser pulse (in picosecond regime) is injected into the medium and collected at some distance from the injection point to count the resulted broadening of pulse. When light is allowed to propagate through a scattering material, it is found that different photons arrive at the detector traveling different distances with different time of-flights (TOF) [1]. This distribution of photon time-of-flights is used to determine the absorption and scattering properties of the sample.
These are the broadened pulses in the turbid medium due to scattering and absorption effect. The higher is the scattering in the medium the wider is the broadening of the pulse.

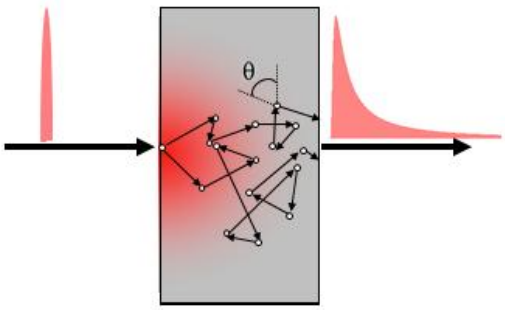

Figure2.1: Light propagation in turbid medium

μ_a : absorption coeff.
μ_s : scattering coeff.
$\mu'_s = \mu_s(1-g)$: effective scattering coeff.
$g \sim \cos^2\theta$

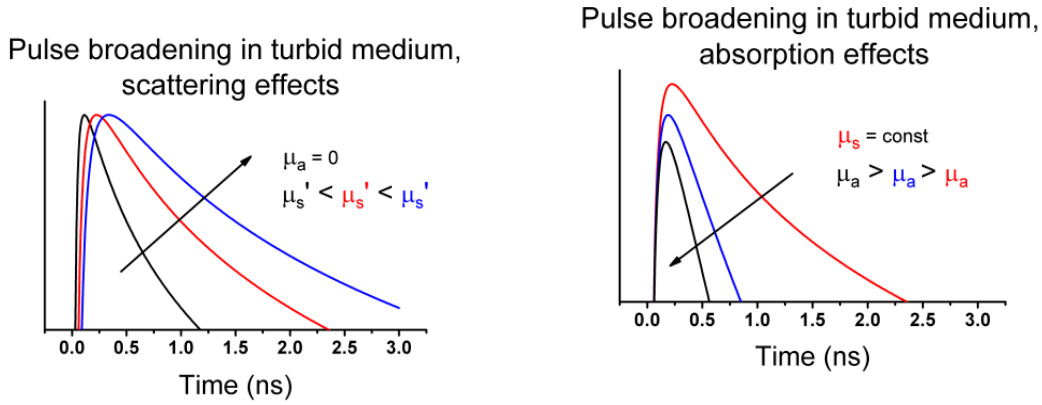

Figure2.2: Pulse broadening in the turbid medium

If the medium is also absorptive then the late photons those travel longer optical paths, have higher probability to be absorbed and as a result the pulse gets narrower. Separately estimated absorption coefficient determines the chemical composition of the material while scattering coefficient tells about the physical or structural properties of the material.

Chapter 3

3. Theory of Photon Migration:

When light enters into a turbid medium, the polarization state and direction of photons becomes randomized due to the multiple scattering events. The photons travel in the form of a random walk. Radiative transfer equation (RTE), also referred to as the Boltzmann transport equation, is very important for describing the propagation of light in turbid media. Solving RTE with the diffusion approximation, transportation of photon in turbid medium can be modeled analytically for some particular geometry. Otherwise, this equation can also be used to simulate the photon transport (Monte Carlo simulation) in a medium of any geometry. In this chapter, the basic theories of the photon migration in the highly scattering media will be discussed and this discussion is based on the publication of **Daniele Contini** et al [2] and **Haskel** et al [3].

The RTE [4, 5] express the balance of energy inside a volume element of the scattering medium. The RTE can be obtained by considering the total space and time variation of the specific intensity along a direction $\hat{s}$ in an elementary volume and making this equal to the variation of specific intensity due to scattering and absorption inside the medium. The final equation for the time dependent case is [6]:

$$\frac{1}{v}\frac{\delta}{\delta t} I(\boldsymbol{r},t,\hat{s}) + \hat{s}\,\nabla I(\boldsymbol{r},t,\hat{s}) = -\mu_t I(\boldsymbol{r},t,\hat{s}) + \frac{\mu_t}{4\pi}\int_{4\pi} p(\hat{s},\hat{s}')I(\boldsymbol{r},t,\hat{s}')d\omega' + \varepsilon\,(\boldsymbol{r},t,\hat{s}) \ldots\ldots (3.1)$$

Where, $I(r,t,\hat{s})$ is the specific intensity or energy, moving in the direction $\hat{s}$, per unit of solid angle, per unit of time, and per unit of area normal to the $\hat{s}$ direction. v is the speed of light inside the diffusing medium, $\mu_t = \mu_s + \mu_a$ is the extinction coefficient with μ_s and μ_a as the scattering and the absorption coefficients respectively. $\varepsilon\,(r,t,\hat{s})$ is the source term and $p(\hat{s},\hat{s}')$ is the scattering function that defines the probability for a photon moving in the direction $\hat{s}$ to be scattered into direction $\hat{s}'$.

There are three types of source functions frequently used for photon migration in turbid medium, as illustrated in Figures 3.1.

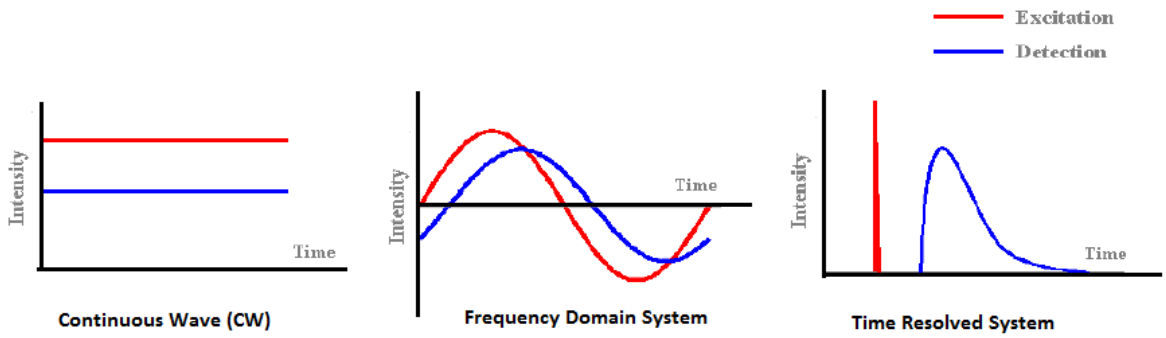

Figure3.1: three types of source functions and relevant systems [7].

For using the continuous wave (CW) light source, the light intensity in the source or the detector is constant. For frequency domain technique, the light intensity is sinusoidally modulated, thus both the amplitude and phase of the sinusoidal wave are counted in measurement. For time-resolved system (TRS), also known as Photon Time of flight system, a short pulse (ps range) is injected and the broadening of the light pulse is recorded. The frequency domain technique and the time domain technique are the Fourier transformation of each other [7].

3.1 Modeling by Diffusion Approximation:

The **RTE** is difficult to solve without introducing approximations. Therefore numerical methods or analytical approximations are often used. The diffusion approximation (DA) can be used to simplify the RTE for some sample geometries such as infinite medium, semi-infinite medium and slab medium. In this modeling only elastic scattering is considered such that the scattering event changes the direction of the photon but does not change its frequency. The absorbed energy is completely lost. To obtain the diffusion equation (DE) in order to build the DA model, source is considered as isotopic that emits a pulse of unit energy $Q(\boldsymbol{r},t) = \frac{1}{4\pi}\delta(\boldsymbol{r}-\boldsymbol{r}')\delta(t)$. The following assumptions are also considered:

1. The specific intensity is assumed to be almost isotropic and is approximated with the first two terms of a Taylor's expansion in terms of the power of $\hat{s}_f.\hat{s}$ [6].

$$I(\boldsymbol{r},t,\hat{s}) = U_d(\boldsymbol{r},t) + \frac{3}{4\pi}F_d\,(\boldsymbol{r},t).\hat{s} \;\ldots\ldots(3.2)$$

Where, $U_d(\boldsymbol{r},t) = \frac{1}{4\pi}\int_{4\pi} I(\boldsymbol{r},t,\hat{s})d\omega$ is called average diffuse intensity and

$F_d\,(\boldsymbol{r},t) = \int_{4\pi} I(\boldsymbol{r},t,\hat{s}).\hat{s}d\omega$ is the diffuse flux vector

2. The phase function $p(\hat{s},\hat{s}')$ is assumed to depend only on the scalar product $\hat{s}.\hat{s}'$.

3. The time variation of the diffuse flux vector over a length of $\frac{1}{\mu_s'}$ is assumed to be negligible with respect to the vector itself.

Now applying the Fick's law,

$$F_d\,(\boldsymbol{r},t) = -4\pi D\nabla U_d(\boldsymbol{r},t) \ldots.(3.3)$$

We can get diffusion equation (DE) for a homogeneous non-absorbing medium is

$$\left(\frac{1}{v}\,\frac{\delta}{\delta t} - D\nabla^2\right)U_d(r,t) = Q(\boldsymbol{r},t) \ldots\ldots..(3.4)$$

Then different solutions of this equation can be obtained including absorption effect for an infinite medium, a semi-infinite medium and slab medium with different boundary conditions. Here these will be discussed only for time resolved system.

3.1.1 Infinite-Medium Solutions to the Diffusion Equation:

The general solution of equation (3.4) for an isotropic source that emits a pulse of unit energy in an infinitely extended homogeneous non-absorbing medium is given by [5]:

$$U_d(\boldsymbol{r},t) = \frac{v\exp(-\frac{|r-r'|^2}{4Dvt})}{4\pi(4\pi Dvt)^{3/2}} \ldots\ldots(3.5)$$

Including absorption effect the solution can also be written for homogeneous scattering and absorbing medium with Eq. 3.5, i.e., by multiplying by $\exp(-\mu_a vt)$

$$U_d(\boldsymbol{r},t) = \frac{v\exp(-\frac{|r-r'|^2}{4Dvt}-\mu_a vt)}{4\pi(4\pi Dvt)^{3/2}} \ldots\ldots(3.6)$$

Where, $D = \frac{1}{3\mu_s(1-g)} = \frac{1}{3\mu_s'}$ is the diffusion coefficient.

When a narrow collimated pulsed light beam, supposed to be thin and collimated pencil beam, is normally incident (along z axis) on the surface of a semi-infinite medium or slab medium, it is assumed that all incident photons are initially scattered at a depth $z_o = {}^1/_{\mu_s'}$ below the surface and the line of sources is thus replaced with a single isotropic source located at z_o into the medium as shown in the figure (3.2) & figure (3.3).

3.1.2 Extrapolated-Boundary Condition:

Extrapolated boundary condition takes proper account of refractive index mismatch at the boundary interface of turbid and transparent mediums. In this boundary condition the average diffuse intensity (fluence rate) is not zero at the physical boundary of the medium rather at an extrapolated boundary located a distance z_e outside the turbid [3, 6].

$$z_e = 2AD \ldots\ldots(3.7)$$

Where, the coefficient *A* is given by

$$A = \frac{1 + 3\int_0^{\pi/2} R(\theta_i)cos^2(\theta_i)\sin(\theta_i)d\theta_i}{1 - 2\int_0^{\pi/2} R(\theta_i)\cos(\theta_i)\sin(\theta_i)d\theta_i} \ldots\ldots\ldots (3.8)$$

θ_i is the angle of incidence of the radiation and $R(\theta_i)$ is the Fresnel reflection coefficient for un-polarized light. If the refractive index (n_2) of the strongly scattering medium and the refractive index (n_1) of bounding transparent medium are substantially different (e.g., n_2 = 1.40 and n_1 = 1.00), a significant fraction of the diffuse flux incident upon the boundary from inside will be reflected back into the turbid medium. This reflected diffuse flux is effectively equivalent to diffuse flux incident upon the medium from outside. Radiant incident from inside at a grazing angle will suffer total internal reflection.

Equation (3.8) is complex but has been fitted by Contini et al. to have the form

$$A_{fitt} = 504.332889 - 2641.00214n + 5923.699064n^2 - 7376.355814\,n^3 + 5507.53041\,n^4 - 2463.357945n^5 + 610.956547\,n^6 + 64.8047n^7 \ldots\ldots (3.9)$$

for $n = n_2/n_1 > 1$

3.1.2.1 Semi-infinite Medium:

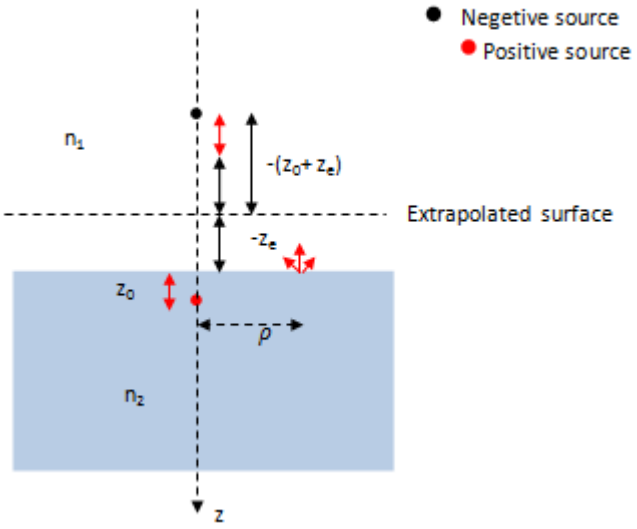

Figure3.2: Semi-infinite homogeneous medium for diffused reflectance. The incident pencil beam is assumed to create an isotropic photon source at depth z_0, indicated by the filled red circle.

For semi-infinite medium the diffused reflectance

$$R(\rho,t) = \frac{\exp\left(\mu_a vt - \frac{\rho^2}{4Dvt}\right)}{2(4\pi Dv)^{3/2}t^{5/2}} \times \left[z_0 \exp\left(-\frac{{z_0}^2}{4Dvt}\right) + (z_0 + 2z_e)\exp\left(-\frac{(z_0+2z_e)^2}{4Dvt}\right)\right] \ldots (3.10)$$

Where,

μ_a = absorption coefficient of the diffused medium

$v = \frac{c}{n_2} =$ velocity of light in the defused medium

$D = \frac{1}{3\mu_s'}$ is the diffusion coefficient.

t = time

ρ = distance of collection fiber from the z axis

3.1.2.2 Slab Medium:

The Positions of source dipoles for slab geometry with extrapolated boundary condition is shown as bellow

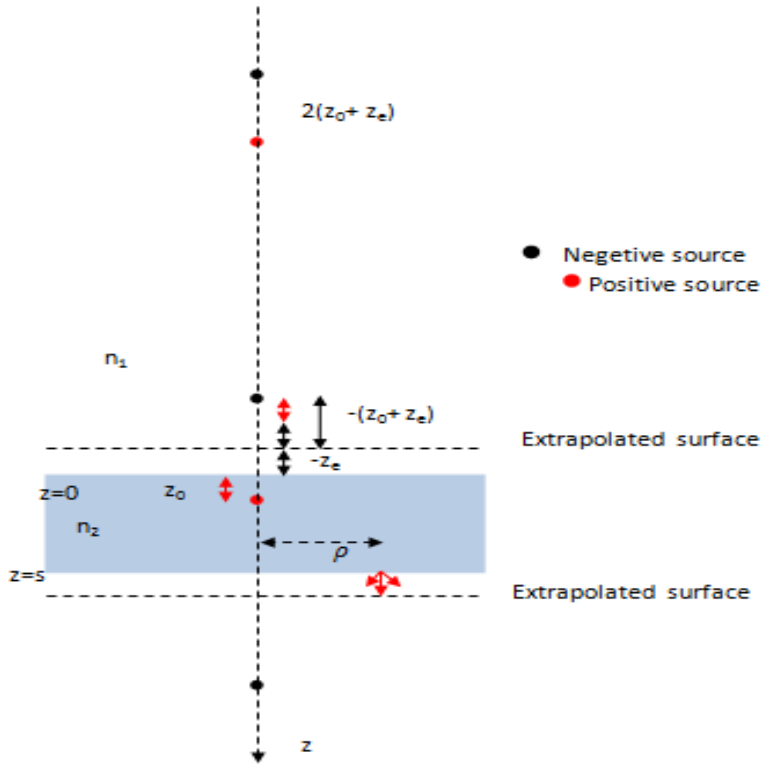

Figure 3.3: Positions of source dipoles for slab geometry

This slab geometry with extrapolated boundary condition is very suitable for measuring the optical properties of real tablets. The diffused reflectance for this geometry is [2]:

$$R(\rho,t) = -\frac{\exp\left(\mu_a vt - \frac{\rho^2}{4Dvt}\right)}{2(4\pi Dv)^{3/2}t^{5/2}} \times \sum_{m=-\infty}^{+\infty}\left[z_{3,m}\exp\left(-\frac{{z_{3,m}}^2}{4Dvt}\right) - z_{4,m}\exp\left(-\frac{{z_{4,m}}^2}{4Dvt}\right)\right] \dots\dots\dots (3.11)$$

And time defused transmittance is [2]:

$$T(\rho,t) = \frac{\exp\left(\mu_a vt - \frac{\rho^2}{4Dvt}\right)}{2(4\pi Dv)^{3/2}t^{5/2}} \times \sum_{m=-\infty}^{+\infty}\left[z_{1,m}\exp\left(-\frac{{z_{1,m}}^2}{4Dvt}\right) - z_{2,m}\exp\left(-\frac{{z_{2,m}}^2}{4Dvt}\right)\right] \dots\dots\dots\dots\dots (3.12)$$

Where,

$$z_{1,m} = s(1-2m) - 4mz_e - z_o$$
$$z_{2,m} = s(1-2m) - (4m-2)z_e + z_o$$
$$z_{3,m} = 2ms - 4mz_e - z_o$$
$$z_{4,m} = -2ms - (4m-2)z_e + z_o$$

And

μ_a = absorption coefficient of the diffused medium

$v = \frac{c}{n_2} =$ velocity of light in the defused medium

$D = \frac{1}{3\mu_s'}$ is the diffusion coefficient.

t = time

ρ = distance of collection fiber from the z axis

$z_o = {}^1/_{\mu_s}$, is the depth below the surface where all incident photons are initially scattered

s = the thickness of the slab

The functions $R(\rho, t)$ and $T(\rho, t)$also represent the probability that a photon, entering the medium at the origin of the coordinate system at t=0, exits at time t and at distance ρ from the z axis per unit of time and unit of area.

Besides extrapolated boundary condition, zero boundary condition (ZBC) and partial current boundary condition (PCBC) are also used for modeling the photon migration in turbid medium. For implementing zero boundary condition, diffusion equation (3.6) is used. However, ZBC assumes diffuse intensity is zero on the surface of the turbid medium. It does not consider refractive index mismatch at the boundary interface. Putting z_e =0 in equation-(3.10), (3.11) & (3.12) it is possible to get diffused reflectance for semi-infinite geometry and diffuse reflectance & transmittance for slab geometry. On the other hand, partial current boundary condition (PCBC) is known as the radiation boundary condition in the context of heat diffusion [8]. The PCBC makes the reasonable assumption that the photons leaving the scattering medium through the scattering & transparent medium interface do not return to the medium. This implies that the total diffuse flux inwardly directed should be equal to zero at the surface. These solutions are rather complex.

3.2 Modeling by Monte Carlo Simulation:

Monte Carlo simulation uses probability distributions to model propagation of light in turbid medium. It is based on the transport equation and had mainly been developed for neutron transport in combination with nuclear reactions. For light transport in turbid media, photons are considered as particles neglecting all wave nature. This method is built on random walk, where a photon or a photon package is traced through the scattering medium until it exits due to scattering or is terminated due to absorption. By repeating this process for a large number of photon packages, it is possible to obtain statistics for these physical quantities.

Although for some geometry, the diffusion approximation can be used to simplify the RTE to model analytically the photon transport in multiple scattering medium, it introduces inaccuracies while scattering coefficients of the medium is not much higher than the absorption or separation between the source and detector is not large in space and time. In

contrast, Monte Carlo simulations can be made arbitrarily accurate by increasing the number of photons traced and its probabilistic solution is not limited concerning boundary conditions or spatial localization of in-homogeneities in the medium. On the contrary, there is a problem of getting good statistics, particularly if the point of interest is located far away from the point of entry of the light and the scattering and absorption coefficients are high.

3.3 Fitting of Experimental Data with Theoretical Model:

The above mentioned models are used to calculate scattering and absorption coefficient from PTOF distribution. Experimentally obtained PFOT distribution is fitted with theoretically modeled curve by fitting algorithms for extracting correct optical properties. For WMC (White Monty Carlo) evaluation of time of flight data, the fitting procedure is based on an exhaustive search over a predefined μ'_s interval with a finite resolution, $\Delta\mu'_s$. For each μ'_s value, the optimal values of μ_a and a free amplitude parameter, *k* are determined using Marquardt-Levenberg minimization of the error norm:

$$\tilde{\chi}^2 = \boldsymbol{min}_{k,\mu_a}\{\chi^2(k, \mu_a, \mu'_s)\ \}$$

Generally, optimum fitting is achieved by minimization of a scalar function χ^2 in fitting algorithm that measures the goodness of fit between the experimental data and the model.

When the diffusion approximation is employed for data evaluation, an optimal fit between experimental data and theoretically modeled curve is reached iteratively by employing Levenberg- Marquardt optimization (in which μ'_s, μ_a and the free amplitude parameter *k* are adjusted). During the iterative data fitting procedure, the impulse response provided by the models is convoluted with the recorded IRF [9].

Chapter 4

4. Instrumental Setup of Wide Bandwidth PTOF Spectroscopy:

Wide-bandwidth photon time-of-flight spectrometer enables getting absorption and scattering spectra of turbid samples in a singularly broad wavelength range from 600 nm up to 1400 nm. As a source, super continuum fiber laser provides spectrally broad light pulse in the wavelength range 500-1850 nm with repetition rate of 80 MHz and maximum optical power > 3mW/nm. The other essential components are- acousto-optic tunable filter(AOTF), GRIN fiber, variable attenuator FVA-3100, optical combiner, attenuating ND filters, single photon counting avalanche photo detector MPD-100 and micro-channel plate PMT's with InP/InGaAsP photo-cathode and computer with a TCSPC card.

The instrumental setup of the spectrometer is shown in the figure4.1.

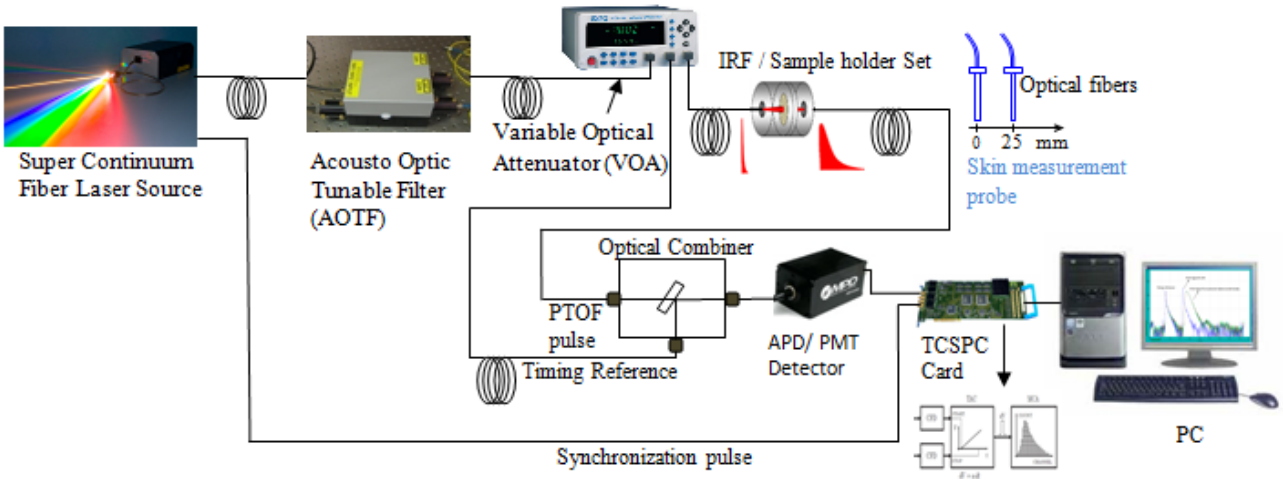

Figure4.1: Setup of Wide bandwidth Photon time of flight spectroscopy (PTOF).

Light pulse from the continuum source is allowed to pass through the acousto-optic tunable filter (controlled by computer) for getting spectrally narrow pulse light of required wavelength. The output of AOTF is connected to a variable optical attenuator (VOA) (controlled by computer) FVA-3100 which controls the power and works as beam splitter. Variable attenuator FVA-3100 has two outputs e.g. “Monitor” and “Output”. “Monitor”

delivers pulse with a very small fraction of attenuated power and it is treated as the timing reference pulse. “Output” delivers pulse with expected attenuated power which is sent to the sample and collected using graded index fiber to get PTOF signal (pulse). Then both the timing reference pulse and the PTOF signal pulse are combined in the optical combiner. This optical combiner is connected with the Photo Multiplier tube (PMT) / Avalanche photo diode (APD) detector for detecting photons. After detecting each photon, detector send signal (electrical response) to Time Correlated Single Photon Counting (TCSPC) electronics which is synchronized with synchronization pulse from the continuum source. Then photon time-of-flight distribution is built and recorded. Measurement can be taken into two different ways, either in reflectance mode or in transmission mode.

4.1 Super-continuum Fiber Laser:

As a light source, Fianum SC-500-6, a pulsed Super-continuum laser with the wide range 500-1850 nm, is used in the setup. This laser source consists of a master source, a high power amplifier, a super-continuum generator and a collimator as shown in figure 4.2.

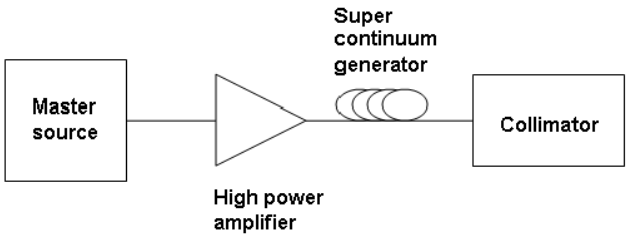

Figure 4.2: Flowchart of the laser components.

The master source consists of a core-pumped, ytterbium (Yb)-doped, low-power fiber laser. It has repetition rate of 80 MHz and generates pulses of 6.0 ps. The master source is coupled to high power amplifier, an Yb-doped fiber with double cladding. This is pumped by a high power laser diode pumping device. Without the amplifier the laser system would only give an output of a few milli-Watts, with a narrow spectral bandwidth centered about 1064 nm. With higher amplification rates both the optical output power and the spectral bandwidth are increased [10].

To generate a broader spectrum a super continuum generator is used. This consists of a highly nonlinear optical fiber, a photonic crystal fiber (pcf). This is a special type of optical fiber with a built-in microstructure where the arrays of holes are arranged in a periodic

manner. By manufacturing the fiber with different holes arrangements, the optical properties of the fiber is changed. The air holes change the fiber's waveguide properties because the refractive index changes with the propagation of light [11]. For the high non-linearity together with the high pulse-peak powers, the spectral range of the pulse is broadened to range from 500 to 1850 nm in the fiber. As the broadening of the spectra is a non-linear process, the spectra will first be extended to longer wavelengths, i.e. greater than 1064 nm which in turn will generate the shorter ones, below 1064 nm. With maximum power to the amplifier, the optical output power is greater than 3mW [12].

4.2 Acousto-Optical Tunable Filter:

In order to get pulse light of narrow band at particular wavelength from the continuum source, Acousto-Optical Tunable Filter is used. This filter consists of a birefringent (double refractive) crystal, which changes its refractive index when it is exposed to an acoustic wave. The filter construction is based on the Bragg condition:

$$sin\theta = \frac{\lambda}{2\,\Lambda}$$

Where, θ is the angle of the incoming light, λ is the wavelength of the light, and Λ is the acoustic wavelength. If both the angle θ and the acoustic wavelength Λ are specified, refection of the incident light can only occur for one single optical wavelength $\lambda = 2\,\Lambda\, sin\theta$. All the other optical wavelengths will be refracted in other directions and will eventually disappear. This wavelength selection property is used to filter desired wavelength.

In this case the refractive index of the crystal is varied by using a piezoelectric transducer to induce an acoustic wave. The continuum light enters the crystal. One wavelength is allowed to be reflected choosing corresponding the acoustic wavelength and from other side of the crystal, the light with the chosen wavelength is collected by a fiber placed in a pinhole. For changing different acoustic wavelength, the frequency of the piezoelectric transducer is changed and controlled by an AOTF-driver, which in turn is controlled through a computer. The radiation from the super continuum fiber laser is spitted over two Acousto Optical Tunable Filters (AOTF) that allow to cut spectrally narrower pulses from the super-continuum. AOTFs deliver

pulses with bandwidth 3-6nm in the range 650nm to1100nm and bandwidth 6-12nm in the range 1100nm to 1850nm [10].

4.3 Variable Optical Attenuator (VOA):

In order to control the super-continuum (SC) laser source power variable optical attenuator (VOA) (controlled by computer) FVA-3100 is used. It can attenuate the power for wavelength range from 650nm to 1000nm up to -100dB and for wavelength range from 1000nm to 1350nm up to -65dB. This variable attenuator box is also act as the beam splitter. First it attenuates and then splits the light. It has two outputs; one is "Monitor" and another is "Output". "Monitor" delivers pulse with a small fraction of attenuated power which is treated as the timing reference pulse. "Output" delivers pulse with expected attenuated power which is sent to the sample to get PTOF signal pulse.

4.4 GRIN fiber:

For transporting light to and from the sample, a graded-index or graded-index fiber of 400 µm core diameter (custom made) is used by matching the fiber aperture with active area diameter of the single-photon avalanche photo-detector (SPAD). This fiber has numerical aperture 0.27. GRIN fiber core has a refractive index that decreases with increasing radial distance from the fiber axis. Therefore the velocity of the light is minimum at the center and increases gradually with radial distance. This type of fiber is very efficient to avoid the temporal broadening of the pulse due to multimodal dispersion.

4.5 The Detectors:

After combining the PTOF signal pulse and timing reference pulse with optical combiner, these are sent to detector. Two types of detectors are used here to cover 600nm to 1400nm region. For 600nm to 1000nm region, we have introduced single-photon avalanche photo diode (SPAD) detector called **PDM100ct** from Micro photon Device. This detector is an APD biased in such a way that the arrival of a single photon precipitates avalanche breakdown, thereby creating a large current pulse that signifies the arrival of a photon. Its photon detection efficiency is about 49% at 550nm and it is obtained through the use of epitaxial

silicon Single Photon Avalanche Diodes with active area diameter of 100µm. Its detection range is from 400nm to 1000nm.

At 1000nm to 1400nm region micro-channel plate PMT (R3809U-68 from Hamamatsu Photonics) with InP/InGaAsP photo-cathode is used. This NIR PMT is extremely sensitive to room light and requires cooling up to -80^{0}C in order to reduce the thermal noise and enhance the sensitivity of the detector. The signal for this PMT is then amplified by amplifier called HFAC-26, Becker& Hickl [13].

4.6 NIR PMT Detector Cooling:

The cooling system for NIR PMT detector is R3809U-50/1406 from Research Inc. For cooling the detector, liquid nitrogen is pumped from a dewar and this pumping is controlled by the temperature. When the detector reaches at required temperature, the pumped liquid nitrogen is released automatically and the temperature remains constant. We prepared an air tight lid (Aluminum ring) for the dewar in such a that no external pressure is required for pumping the nitrogen.

4.7 Holder Set for Measuring Sample and IRF in Transmission Mode:

For measuring the tablet shaped sample and IRF in transmission mode, new type of holder set was prepared with lens tube of 1" thread depth, two FC/PC fiber adapter plates and sample holder.

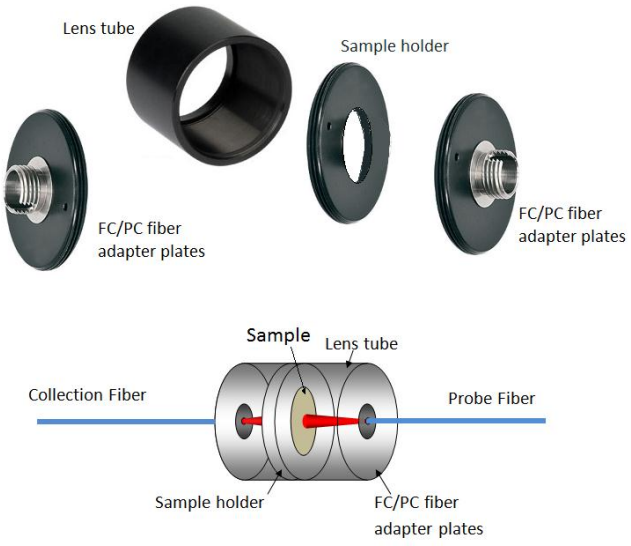

Figure 4.3: Holder Set for Measuring Sample and IRF in Transmission Mode.

For this holder, the fibers with FC/PC connectors can be used directly for probe and collection. The probe and collection fibers remain perfectly aligned and the possibility to break or scratch the fiber tips becomes quite less. As, the fiber tip does not touch the surface of the sample or IRF, it does not destroy the IRF black paper and increases the stability for measurements.

4.8 Time-correlated Single Photon Counting Technique:

Time-correlated single photon counting (TCSPC) technique is very efficient for sensitive detection and high time resolution and is based on the detection of individual photons. A fast detector delivers signals corresponding to single photon detection events. The time stamp of a photon detection event is measured with respect to a reference pulse from the light source. Here, as TCSPC card SPC-130 from Becker & Hickl was used.

In TCSPC experiments, it always involves repeated injection and detection and counts timing of zero or one photon from each period (pulse). The technique is thus not capable of handling the detection of several photons at each signal period as it is difficult to measure accurate timing of a stream of closely spaced events [14]. The repetitive character of the measurement allows the build-up of a TCSPC photon histogram i.e. a photon time-of-flight distribution.

Principally, TCSPC technique relies on counting very weak optical signal. The signal should be so weak that it is rare to see any photon at all. This is due to that only the first detected photon for each period (pulse) can be noted and analyzed. If the probability for detection of two or more photons per period is not negligible, late photons are discriminated. This result in a statistical error is known as photon pile up. In order to avoid this problem the probability of detection of one photon per pulse is maintained below 1%. Instead of acquiring the overall photon distribution, the technique now generates a histogram describing the distribution of the earliest photon. In the limit of low detection rates, these two distributions are equal. In cases with higher light intensities, the optical signal must be attenuated before it reaches the detector. In practice, this means that it is only a small fraction of the injection

pulses that produce a detection event. Using high repetition-rate pulsed lasers still allow fast generation of proper histogram [14]. A schematic of a typical TCSPC chain is shown in the following figure4.4.

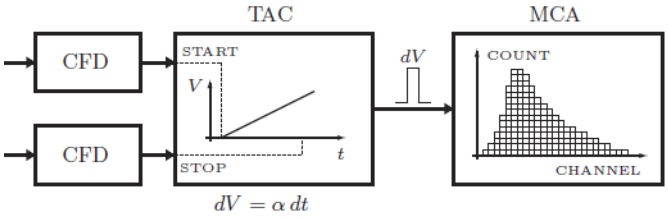

Figure4.4: A schematic of a typical TCSPC setup.

A fast detector (PMT / APD detector) provides pulse (electrical response) for individual photon detection from sample signal. And then send to a Constant fraction discriminator (CFD). A second CFD is also used to obtain a synchronization pulse from the light source. To avoid fluctuation in amplitude in the signals, CFD are used. They improve timing by compensating variation in amplitude and create threshold for noise by rejecting pulses with high and low amplitudes [13]. The output pulses of the CFDs are sent to Time to amplitude converter (TAC) and used as start and stop pulse for internal clock of TAC. Pulse of single detected photon starts the clock and pulse from the source, SYNC, stops the clock. The output from the TAC is an electric pulse with an amplitude proportional to time difference between the start and stop pulse. Conventional TACs use a switched current source charging a capacitor. The start pulse switches the current on while the stop pulse switches it off.

The voltage (proportional to time difference) is then sent to multichannel analyzer. By repeating this procedure several times a statistical histogram is created which represent a photon time-of-flight distribution. That means, the no. of photons is distributed at different time channels where each photon detected from a particular sample pulse.

4.9 IRF Measurement:

The instrumental response function (IRF) describes how the measurement is affected by the instrumental setup. The experimentally measured photon distributions are fitted with the theoretically modeled pulse for evaluation of absorption and scattering. In theory, pulse broadening is modeled assuming that the injected pulse is like a delta function. However, in reality it is not possible to get such laser pulse. As a consequence, this laser pulse with finite width (picoseconds regime) affects the ideal condition for the measurement. Again this pulse

can be dispersed and broadened by fibers, detector or any part of the instrument but not from sample and this may also affect measurements. To circumvent these all effects, IRF measurement is taken to include all broadening in theoretically model pulse. IRF measurement is taken without any sample in such a way that perturbation, caused by the setup, remains the same as the measurement with sample. Then the theoretically modeled pulse is convoluted with IRF and fitted with experimentally data using fitting algorithm. Again, in practical the proper IRF measurement is also complicated because modes of the light, which are filled in detection fiber, are also dependent on the scattering of the sample. That's is why IRF should be measured using such an object that causes very small temporal broadening but still can fill the same modes at the detection fiber as a sample [13]. A thin piece of paper (80 gram), printed black (with maximum contrast) two times each of the both sides, can be useful for preparing this object because paper has scattering that mimic the sample and causes very small temporal broadening for its very small thickness. In our IRF measurement, the pulses of the source with expected power (output of the variable attenuator) were allowed to pass through this thin black printed paper.

4.10 Measurement Procedure & Data Evaluation:

The measurements procedure and the evaluation of the optical properties μ_a and μ_s' can be summarized as:

- Sample (human tissue or pharmaceutical tablets or any turbid media) is placed between the laser source and the detector through probe and the collection fiber for getting broadened pulse (experimental data).
- Instrumental response function (IRF) measurement is taken through the same path.
- For data evaluation, Optimal fit between experimental data and theoretically modeled curve is reached iteratively by employing Levenberg- Marquardt optimization and putting proper guess of μ'_s and μ_a. During the iterative data fitting procedure, the impulse response provided by the models is convolute with the

recorded IRF. Theoretically broadened pulses are modeled using Diffusion approximation or Monte Carlo simulations

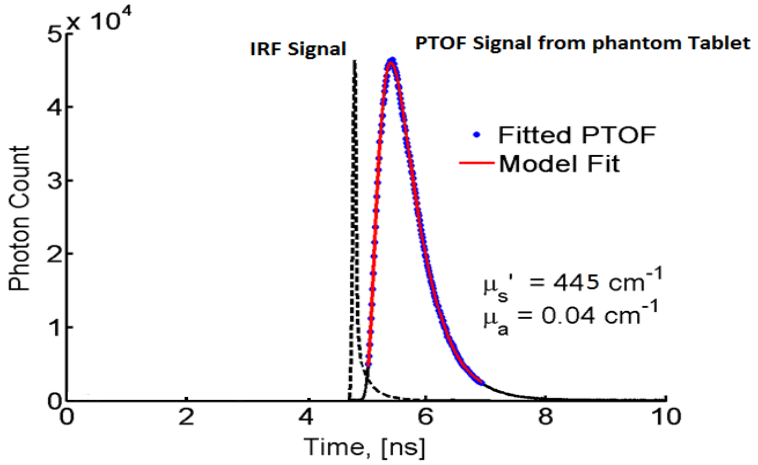

Figure4.5: IRF and temporal distribution of PTOF measurements using TCSPC.

- When scattering is quite high comparing with the absorption in the medium and the separation between the probe and the collection fiber is large, the photon diffusion model is suitable for evaluation of the PTOF data. On the other hand, if the difference between absorption and scattering is not large or the fiber separation is small then the analytical photon diffusion is not applicable. In such conditions for the data evaluation, an advanced data fitting algorithm base on Monte Carlo simulations is used.

Chapter 5

5 Optimizing the Instrumental Setup for Measurement with High Precision:

For different applications of PTOF system, it is very important to maintain high precision in measurement along with accuracy. Accuracy represents the degree of closeness of measurements of any quantity to quantity's actual (true) value while precision of a measurement system is the ability to produce same result repeatedly [15].

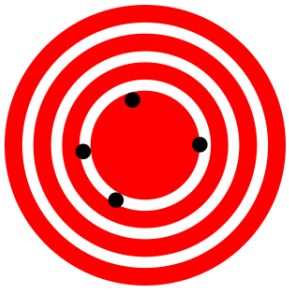

5.1 High accuracy, but low precision [16].

5.2 High precision, but low accuracy [16].

In this spectroscopy, the precision of the measurements heavily depends on precise timing calibration of the system and accurate determination of the instrumental response function (IRF) [17]. In this system, the first problem was observed in the light source. It is good but not sufficiently stable. Here, single-photon avalanche photo diode (SPAD)/PMT detector is used which produces countable electrical pulses in response to single incident photons. In any such detector, there is a random delay from the time a photon is incident on the detector to the time an electrical output pulse is produced in response to that photon [18]. The uncertainty introduced by the apparent source and detector temporal drifts and finite resolution of the TCSPC detection, results error in measurement and leads to poor precision. To observe the nature of temporal drift in the system, continuous measurements of IRF were taken for more than one hour and each measurement took 24 seconds. Then, it was found that the temporal peak position of the IRF (pulse) on the TCSPC channel axis does not remain always at same point rather it is drifting about 2ps per hour in random manner.

This randomness is illustrated in the following fugure-5.1.

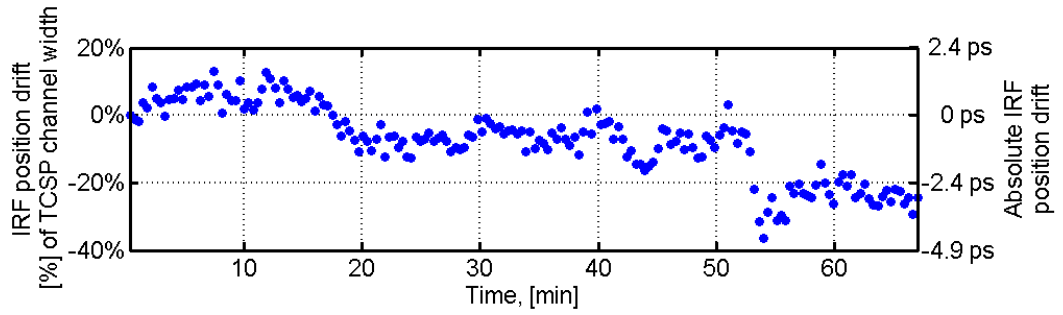

Figure5.2: IRF position drifts with time.

This randomness at peak position of IRF / PTOF signal or both IRF and PTOF signal affects the accurate measurements and provides uncertainties in evaluation of correct optical properties of any samples. From calculation it is observed that for temporal shift of IRF signal with in ± 6ps (TCSP channel axis), the resulted errors are **±6.3%** for absorption coefficient, μ_a **= 0.0395 cm^{-1}** and **±2.3%** for Reduced scattering coefficient μ'_s **=430cm^{-1}.** These are shown below:

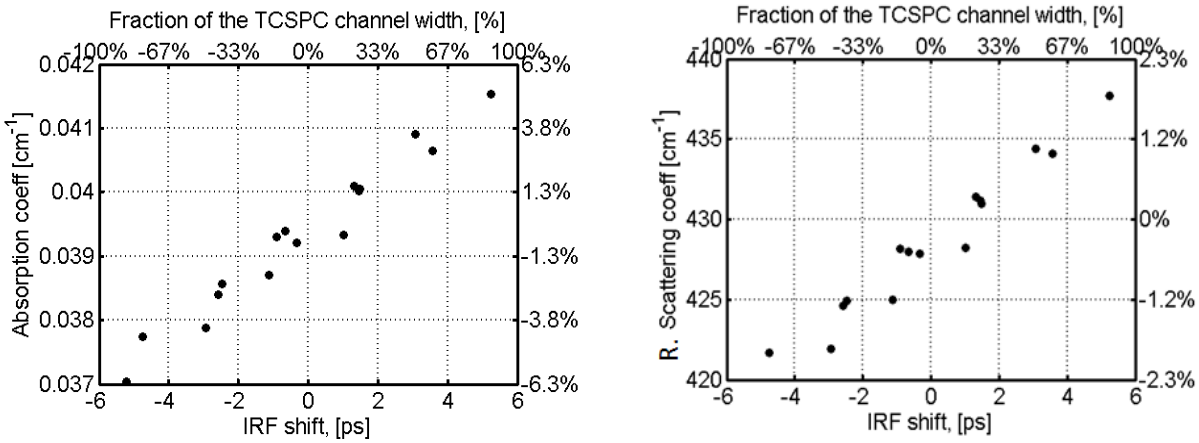

Figure5.3: Errors in μ_s' and μ_a due to IRF temporal drifts.

For getting extremely high precision in measurements, the broadened PTOF signal pulse and the instrumental response function (IRF) must be measured with the certainty of having no temporal drift of jitter in the system. However, in reality it cannot be removed completely. For minimizing it one approach can be to take IRF measurement each time with sample measurement. Again, it is not feasible in many cases, like clinical measurements due to time synchronization and also does not provide much improved results.

To overcome the problem, we have introduced a new idea to measure the fraction of direct laser pulse simultaneously with the IRF and the PTOF signal. This fraction of direct laser pulse is treated here as timing reference signal. The reason for adding this new pulse is that with the PTOF and IRF signal, it is not possible to count the exact temporal drift between these signals for particular measurement as peak of the PTOF signal is completely indeterminable. On the contrary, the timing reference pulses for PTOF signal and IRF pulse must have exactly the same shape and ideally their peaks should come exactly at the same point if there is no jitter in system. So, the difference between their peak positions must reflect the temporal shift in measurement.

Pointing the peaks of timing reference pulse for IRF and timing reference pulse for PTOF signal, now it is very easy to calculate temporal shift in measurements or drift in PTOF signal and IRF pulse correctly. Then this calculated value can be subtracted or added in the software **TimeResolved_v3** to get correct position of the IRF and PTOF signal pulse and measure correct absorption (μ_a) and scattering coefficients (μ_s').

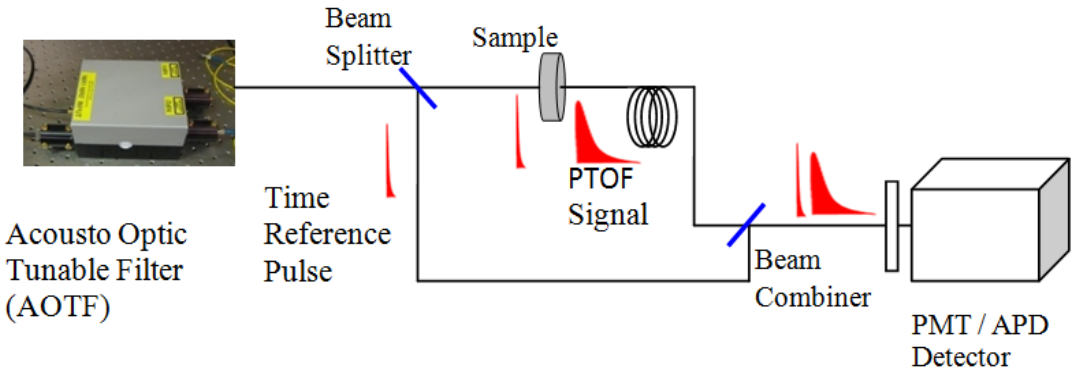

Figure5.4: Introduction of Double Path Optical Scheme.

To implement this whole idea, a new double path optical scheme was added in the setup (see figure5.4) introducing a beam splitter and a beam combiner. As a timing reference signal, a small fraction (low intense) of the splitted direct laser pulse is routed over the dedicated optical path towards the detector using beam combiner where it is superimposed over the PTOF or IRF signals (figure5.5) [17]. The amplitude of the timing reference and its time delay with respect to the signal are controlled via dedicated attenuator and by the length of the reference optical path, respectively.

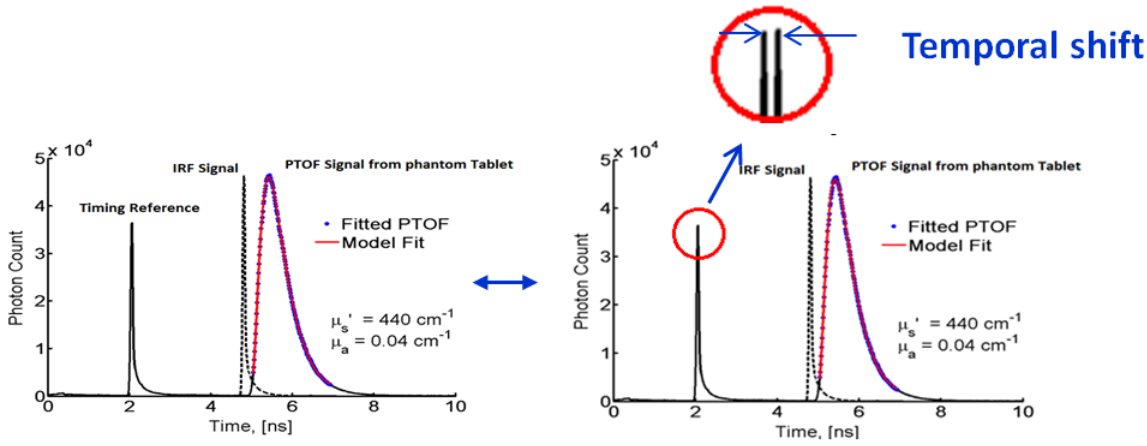

Figure5.5: PTOF signals from phantom tablet and IRF with Timing Reference to visualize signal to noise ratio.

Implementation of the timing reference pulse brings possibility to measure the scattering and absorption properties of the turbid media with high precision (uncertainty less than 1%). To observe the precision in measurements, single measurement for IRF and 180 continuous measurements for same Epoxy Tablet phantom made of TiO_2 and Bg36 chased powder were taken in transmission mode at particular one wavelength 795nm. Then, the optical properties of the phantom were estimated by the evaluation algorithm based on diffusion approximation model assuming refractive index=1.5. It was found that for the timing reference pulse, uncertainty in reduced scattering coefficients (μ_s') reduces from ±1.7% to ± 0.5 % and in absorption coefficients (μ_a) reduces from 2.2 % to ± 0.5 % which is illustrated in figure5.4.

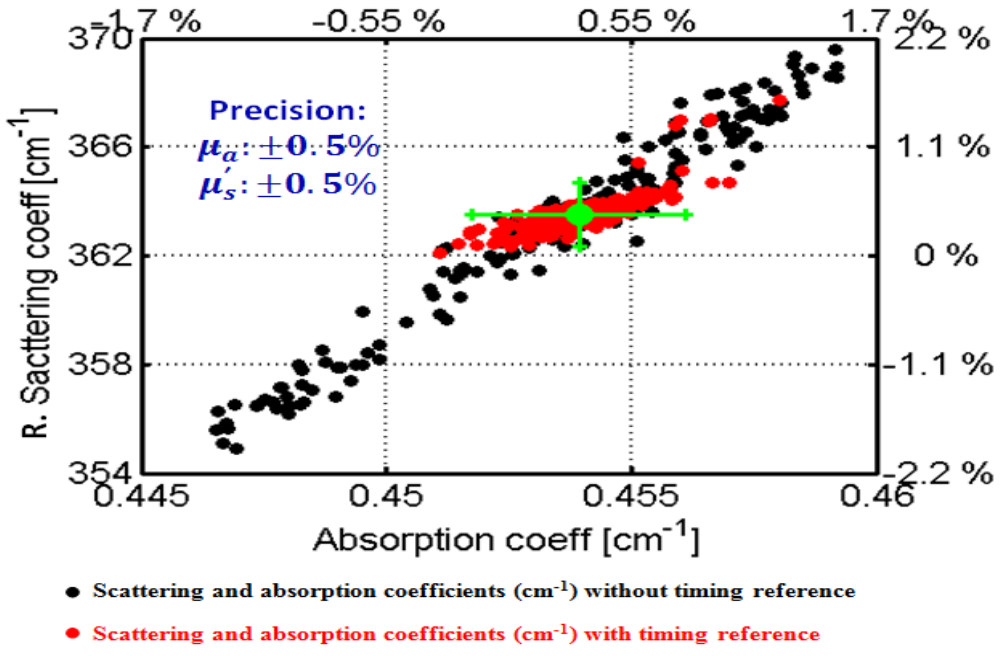

Figure5.6: Showing the measured values of scattering and absorption coefficients (cm^{-1}) with the implementation of timing reference and without timing reference at 795nm.

Then the phantom tablet was measured at two wavelengths 740nm & 800nm for five days to observe the day to day variations in measurements and calculate error in precision. At each day, around 12-16 measurements were taken for IRF and sample. From five days measurements, it is found that at 740nm the reduced scattering coefficients (μ_s') is 335.6 ± 0.3 % and absorption coefficients (μ_a) is 0.38 ± 0.5 % and at 800nm the reduced scattering coefficients (μ_s') is 310.1± 0.2 % and absorption coefficients (μ_a) is 0.46 ± 0.5 %. These results are shown below:

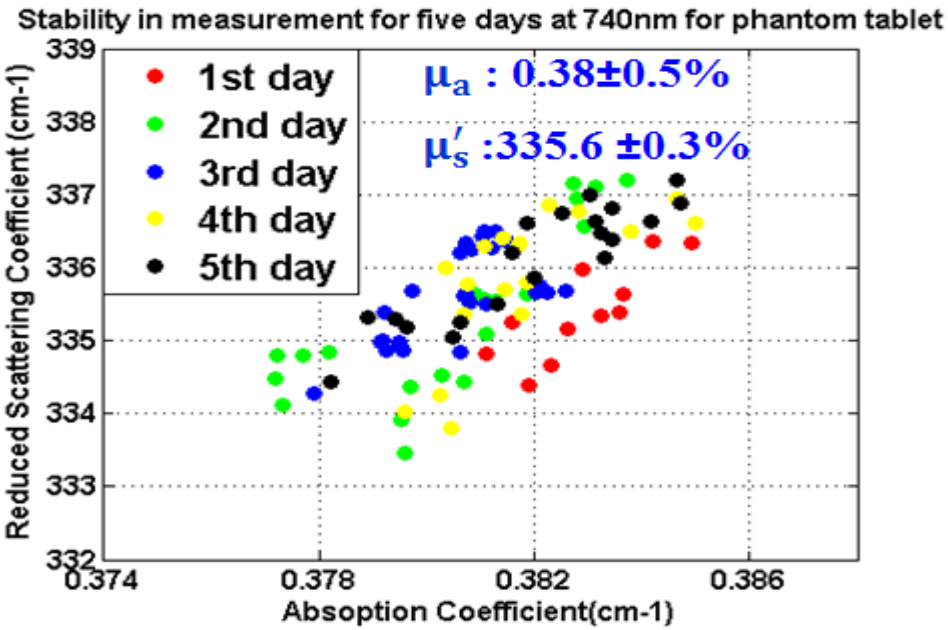

Figure5.7: Stability in measurement for five days at 740nm for phantom tablet.

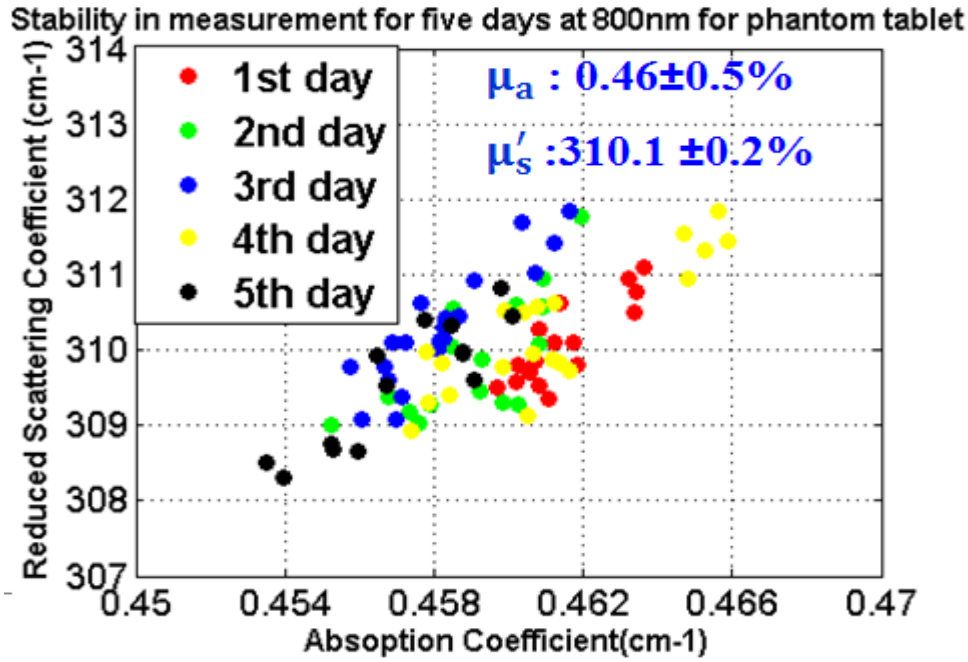

Figure5.8: Stability in measurement for five days at 800nm for phantom tablet.

Chapter 6

6 Phantoms & Experiments for Calibration and Performance Assessment of the System:

PTOF system is a complete combination of optical instruments for measuring optical properties of turbid medium considering light propagation inside the medium. We have replaced detector and optical fiber with SPAD detector & Grin fiber of core diameter 400 µm in the system and introduced double path optical scheme for adding timing reference pulse with IRF and PTOF signal. It is very essential to calibrate this system and assess its performance. In order to do so we have prepared different type of water based and solid phantoms.

6.1 Performance Assessment with Liquid Based Phantoms:

For accurate calibration and performance assessment of the system, experiments were performed on diffusive liquid phantoms based on Intralipid as scatterer and Indian ink as absorber. Intralipid 20% and India Ink solution used for the study were provided by Prof. Giovanni Zaccanti, Dipartimento di Fisica, Universita' degli Studi di Firenze as this work was a part of multi-laboratory study on the accurate calibration of the components for diffusive liquid phantoms.

6.1.1 Liquid Based Phantoms Preparation:

Liquid phantoms are basically water solutions of a diffusive medium. In our experiments phantoms were prepared with Intralipid-20% (Fresenius Kabi Italia, Italy) and pre-dilution of Indian ink (Higgins Waterproof Black India Ink, Sanford, USA). Intralipid is a lipid suspension used for nutrition of hospitalized patients. Diluted ink solution was prepared by mixing 3.7818g ink with 500g water maintaining the ink concentration, c= 0.0075068 [19]. For preparing phantoms and perform experiments, water was kept in a cylindrical plastic container having diameter of 110 mm and height of 120 mm. Then required amount of

Intralipid and pre diluted ink solution were poured and mixed with water by placed container on a magnetic stirrer.

6.1.2 Accuracy & Linearity Verifying Experiment:

Two measurement series were performed: one with added absorber in a step-wise manner, [20] and another one with added scatterer also in a step-wise manner [21, 22], to verify the linearity in performance. As absorber and scatterer diluted ink solution and Intralipid were used respectively. Then, Reduced scattering coefficient of pure Intralipid 20% and absorption coefficient of pre-diluted ink solution (with ink concentration, c= 0.0075068) were determined by extrapolating absorption/scattering values obtained in these added solution series experiments. These experiments were done at low Ink/ Intralipid concentrations and each experiment was performed twice to observe the precision in measurements.

The experiment with added absorber series was performed on a phantom mixing 24ml Intralipid with 700 ml water and adding ink solution with increment of 1 ml in the solution of Intralipid up to 16 ml. On the other hand, the experiment with adding scatterer series was performed on a phantom with 700 ml water without mixing any ink solution and adding Intralipid from 6 to 39 ml with the steps of increment of 3 ml. All measurements were taken at three wavelengths e.g. 751nm, 833nm & 916nm and in all measurements; the probe & collection fibers were placed in parallel at 41 mm depth in the center of the phantom, separated by ρ= 20 mm, center to center. For each measurement, data acquisition was performed for 24 seconds and IRF was measured before and after the completion of measurements in order to monitor the temporal drift. Scattering and absorption coefficients were evaluated using data evaluation algorithm based on White Monte Carlo model [23]. For the evaluation, we assume the following parameters: scattering anisotropy factor g = 0.7 and Intralipid solution refractive index 1.33.

The results from added absorber series (first experiment) are shown in figure below:

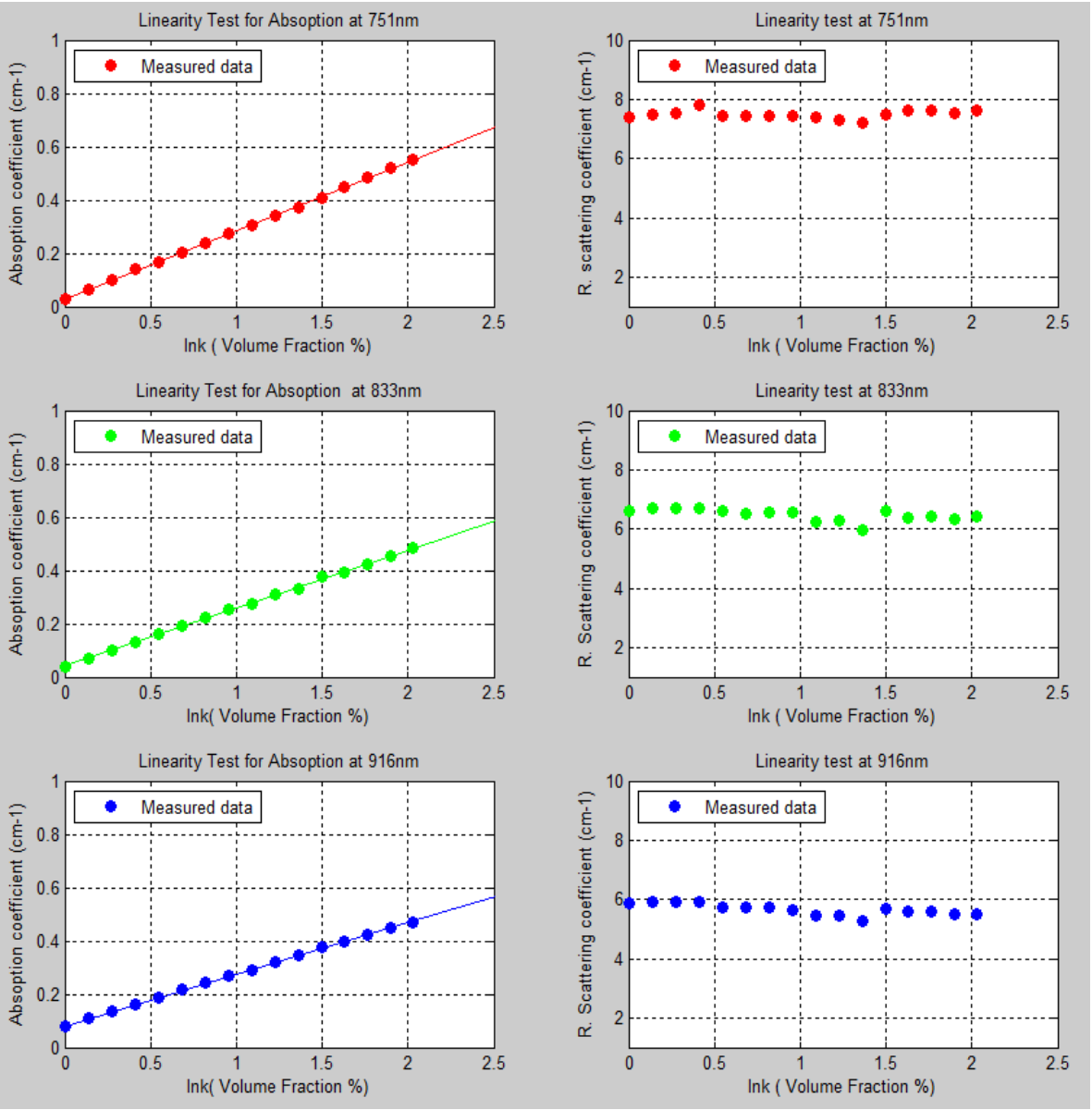

Figure6.1: Linearity of μ_a for absorber series for 1st measurement at wavelengths 751nm, 833nm & 916nm.

During measurements for absorber series, the volume fractions of diluted ink solution increases while the volume fraction of the Intralipid decreases. Considering these both volume fraction changes, it was found that the absorption coefficient (μ_a) increased quite linearly with increasing the amount of absorber Ink while the reduced scattering coefficient (μ_s') decreased slightly. However, by normalizing the scattering values it could be shown that they were quite consistent. Then, by extrapolating the absorption values obtained on a

series measurement with ink solution volume fractions from 0.55% to 2.03 %, absorption coefficient for ink solution (with ink concentration, *c*= 0.0075068) was also evaluated.

The estimated values are as follows:

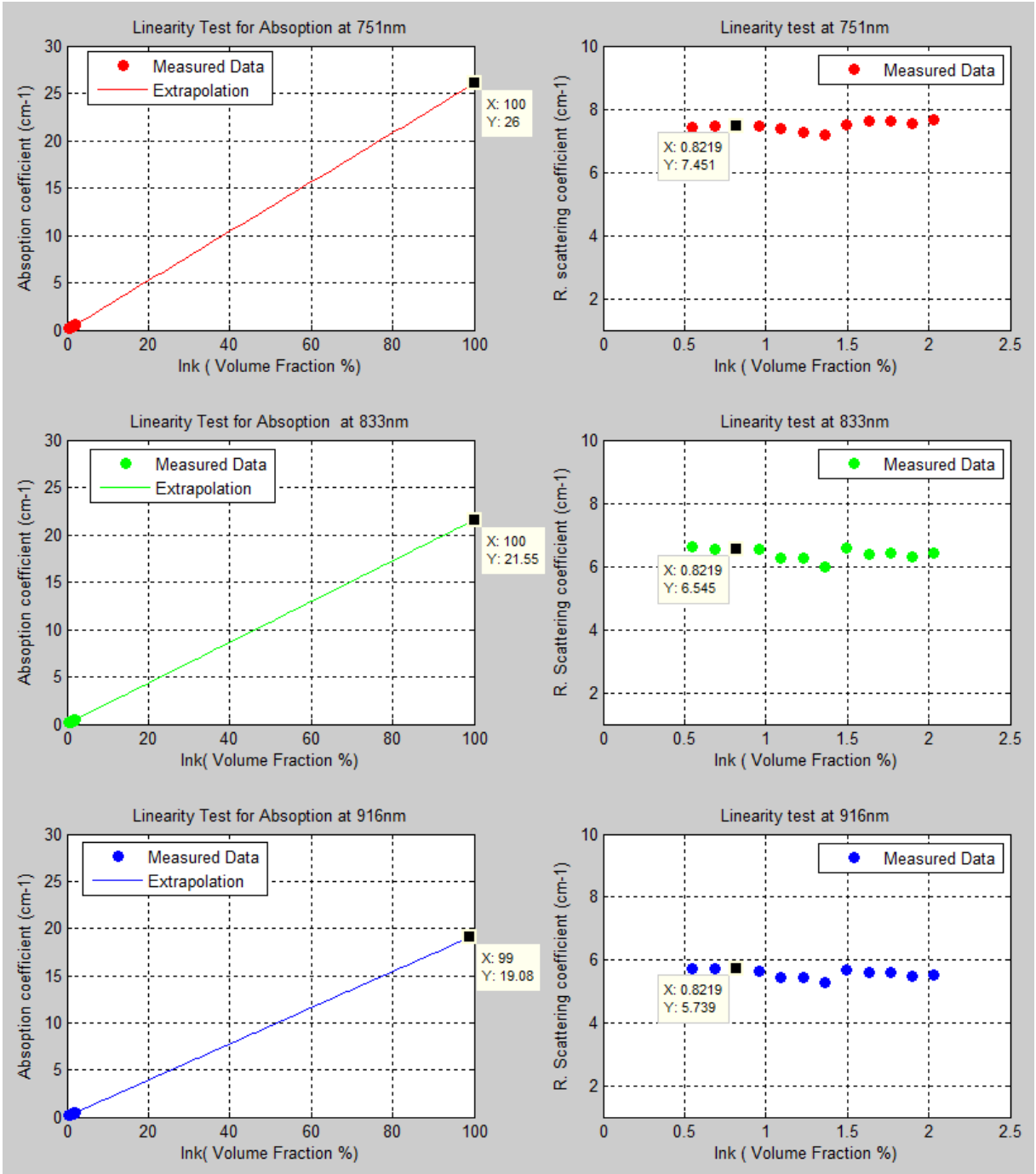

Figure6.2: μ_a for ink solution by extrapolation for for 1st measurement at wavelengths 751nm, 833nm & 916nm.

The evaluated absorption coefficients of ink solution (with ink concentration, *c*= 0.0075068) at different wavelengths from 2nd experiment with added absorber series are shown in figure6.3.

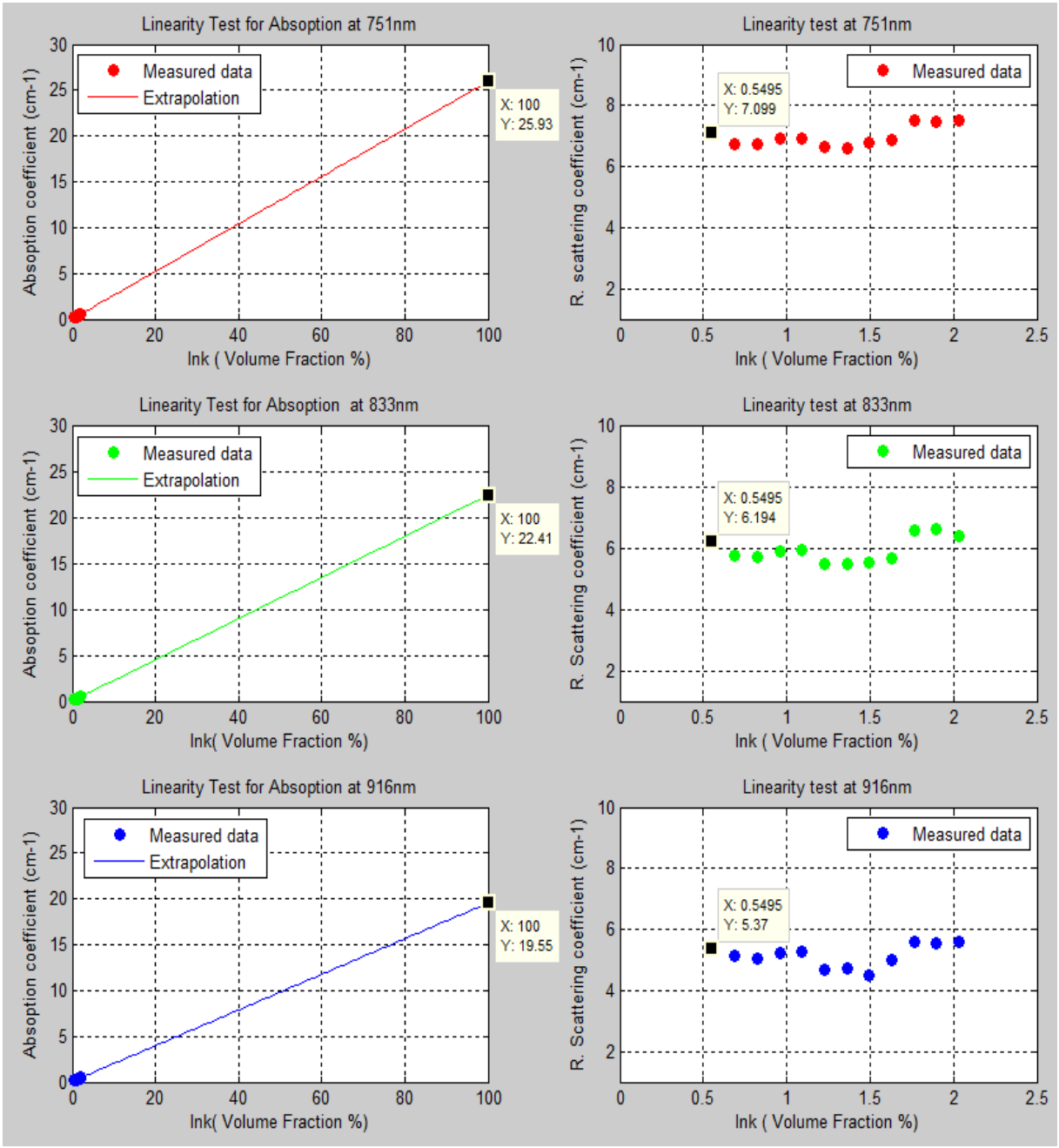

Figure6.3: μ_a for ink solution 20% by extrapolation for 2nd measurement at wavelengths 751nm, 833nm & 916nm.

The results from added scatterer series (first experiment) are shown in the figure6.4.

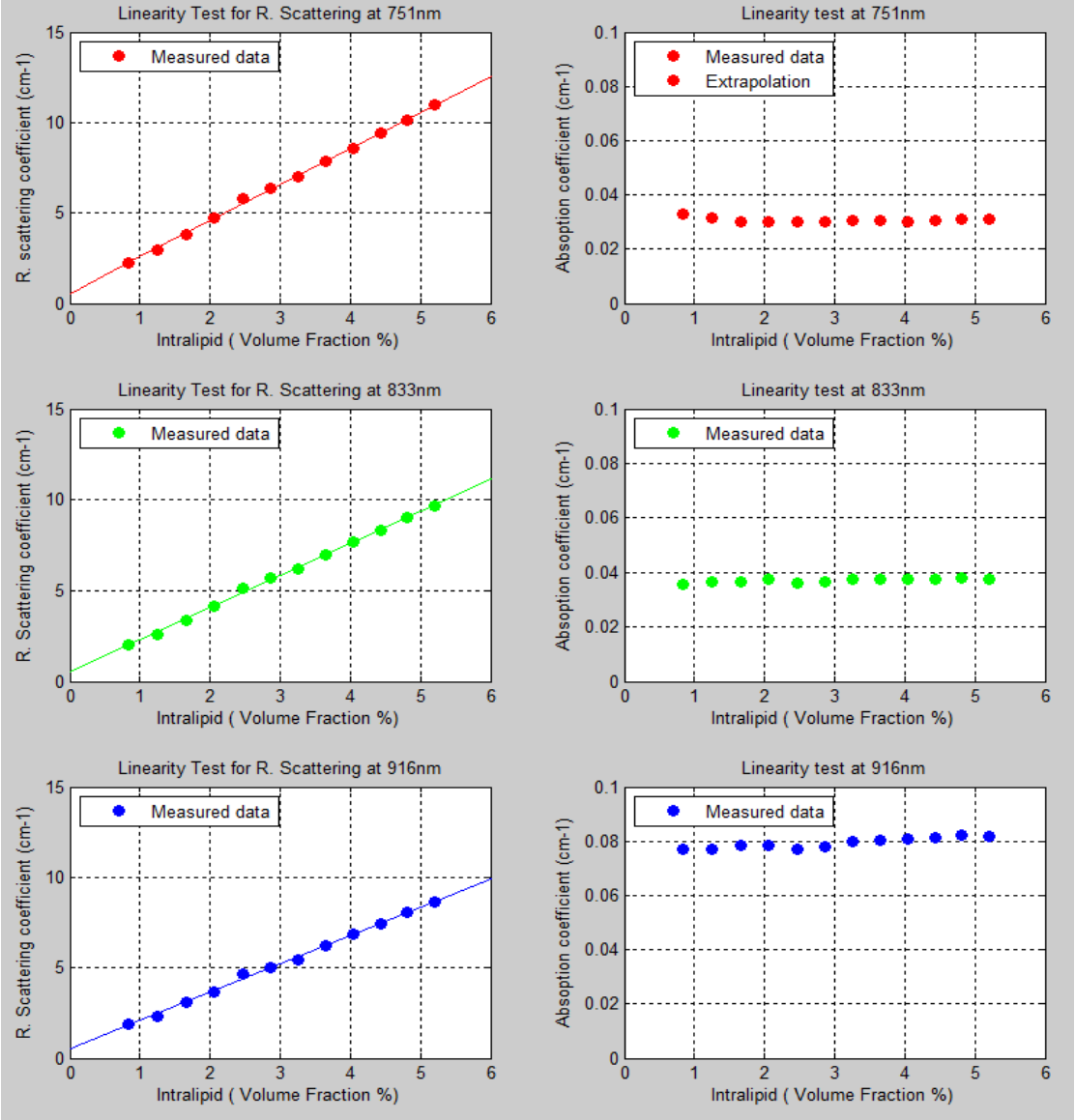

Figure6.4: Linearity of μ_s' for Intralipid series for 1st measurement at wavelengths 751nm, 833nm & 916nm.

In this case of the scatterer series, volume elements of added Intralipid also cannot be neglected as the quantities (from 3 to 39 ml) are comparable to the volume amount of water. So, for scatterer series the volume fractions of Intralipid increases while the volume fraction of the water (only absorber) decreases. Counting these both volume fraction changes, it was found that the reduced scattering coefficient (μ_s') increased quite linearly while the absorption coefficient ($\boldsymbol{\mu_a}$) decreased slightly. Then, by normalizing the absorption coefficient values it was found that they were quite consistent. Then, by extrapolating scattering coefficients values obtained on a series measurement with Intralipid volume

fractions from 0.84% to 5.3%, reduced scattering coefficient of the pure intralipid was measured and shown in the figure:

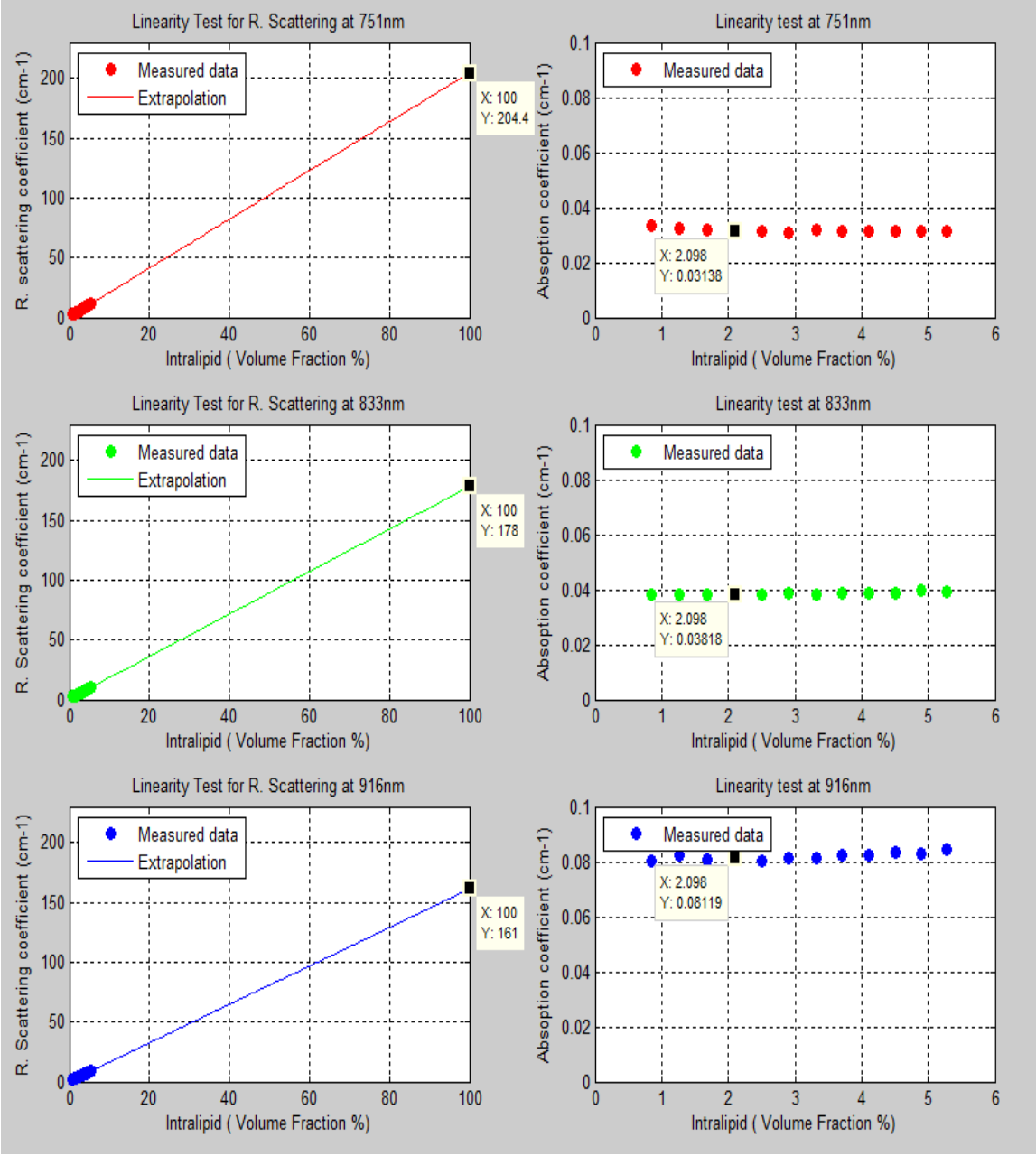

Figure6.5: μ_s' for Intralipid 20% by extrapolation for 1st measurement at 751nm, 833nm & 916nm.

From second experiment with added Intralipid series, the evaluated absorption coefficients of pure Intralipid at different wavelength are shown in figure6.3

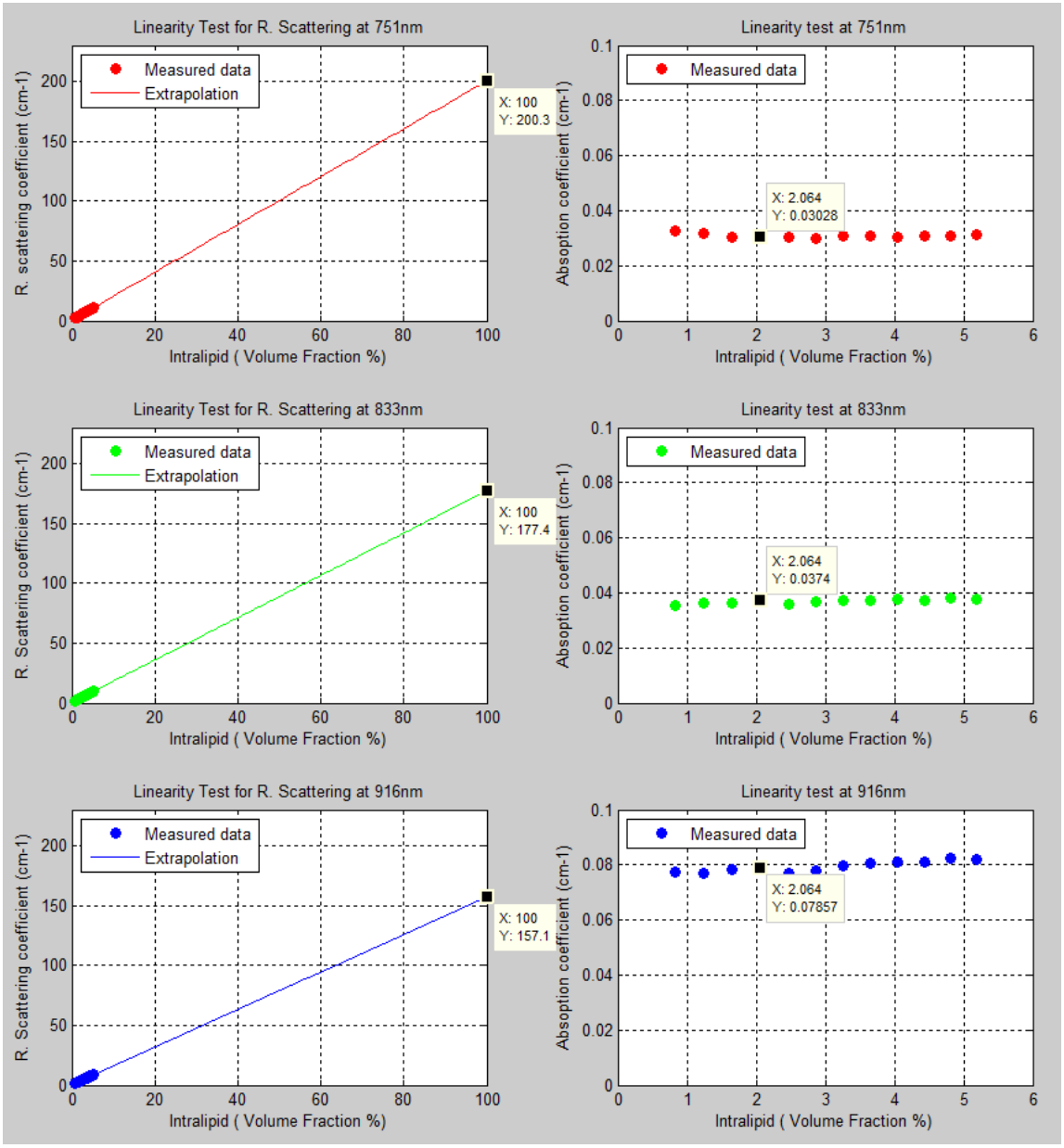

Figure6.6: μ_s' of Intralipid 20% by extrapolation for 1st measurement at 751nm, 833nm & 916nm

6.1.3 Results:

The estimated absorption coefficients of ink solution and reduced scattering coefficients of Intralipid 20% at different wavelengths are reported in Tables 6.1and 6.2.

Table6.1: Reduced Scattering Coefficient (μ_s') of Intralipid-20

	First Measurement	Second Measurement	Average	90% Confident Interval	Difference % 1^{st} mes.-2^{nd} mes.	Error for $\Delta\rho$ =5%	Reference value [18].
μ_s' (cm^{-1}) at 751nm	204.4	200.3	202.4	±1.3%	2.03 %	10 %	208±3%
μ_a (cm^{-1}) at 751nm	0.031	0.0303	0.0307	±2.2%	2.3 %	0.7 %	
μ_s' (cm^{-1}) at 833nm	178	175.6	176.8	±1.4%	1.4 %	9.5 %	188±0.7%
μ_a (cm^{-1}) at 833nm	0.038	0.037	0.0375	±2.4%	2.6 %	2.7 %	
μ_s' (cm^{-1}) at 916nm	161	157.1	159.05	±1.5%	2.5 %	9.4 %	
μ_a (cm^{-1}) at 916nm	0.081	0.079	0.08	±2.6%	2.5 %	1.3 %	

Table6.2: Absorption Coefficient (μ_s') of Ink solution (with ink concentration, *c*= 0.0075068).

	First Measurement	Second Measurement	Average	90% Confident Interval	Difference % 1^{st} mes.-2^{nd} mes.	Error for $\Delta\rho$ =5%	Reference value.
μ_a (cm^{-1}) at 751nm	26	25.93	25.97	±1.1%	0.26%	2.6 %	27.75
μ_s' (cm^{-1}) at 751nm	7.5	7.1	7.3	±2%	5.2%	10.1 %	
μ_a (cm^{-1}) at 833nm	21.55	22.18	21.87	±1.7%	21.9%	6.2%	24.56
μ_s' (cm^{-1}) at 833nm	6.6	6.2	6.4	±3%	6.4%	13.2 %	
μ_a (cm^{-1}) at 916nm	19.27	19.35	19.3	±1.9%	19.5%	2.8%	
μ_s' (cm^{-1}) at 916nm	5.7	5.4	5.6	±3.4%	5.6%	9%	

Table6.3: Absorption Coefficient (μ_s') of pure Ink.

	Result for ink solution with ink concentration, *c*= 0.0075068	Reference value.	Result for pure ink	Reference value [18].
μ_a (mm^{-1}) at 751nm	2.597±1.1%=2.597±0.028	2.775±0.030	345.95±3.7	319
μ_a (mm^{-1}) at 833nm	2.187±1.7%=2.187±0.037	2.456±0.025	291.3 ±4.92	289
μ_a (mm^{-1}) at 916nm	1.93±1.9%=1.93±0.037		257.1±4.92	

In the present study random experimental errors in determination of absorption/scattering coefficient of ink solution/ Intralipid occurred due to uncertainties in added solution volumes and residual fitting uncertainty due to finite signal to noise ratio in acquired time-of-flight characteristics. Besides, the factor which dominates to produce errors is the uncertainty in the distance between probe and collection fibers. Taking account of realistic uncertainty in inter-fiber separation (Δρ) of ±0.5mm, the variation in absorption/scattering coefficient of ink solution/ Intralipid were estimated by the evaluation algorithm assuming inter-fiber distance of 19.5nm and 20.5mm in order to count the systematic error. The analysis shows that 5% uncertainty in fiber positioning results approximately 10% uncertainty in determination of reduced scattering of Intralipid and 2.5% uncertainty in determination of absorption coefficient of ink solution. The scattering systematic error estimation also follows form the condition $\mu_s'\rho^2 = const$, which suggests that scattering error in % is twice of that in inter-fiber separation ρ.

Student's t-distribution yields the following evaluation of the 90% confidence interval for scattering/absorption coefficients estimated in the present study:

$$\mu \pm A_n^{90\%} \frac{\sigma_\mu}{\sqrt{n}}$$

Here, μ is estimated value, n number degrees of freedom ($n = 10$ for 11 experimental values), σ_μ unbiased estimation of the standard deviation, $A_n^{90\%}$ Student's t-distribution parameter ($A_{10}^{90\%} = 1.81$) [24].

6.2 Performance Assessment with Solid phantoms:

Extremely good accuracy and high precision in the measurements are prime need for precise evaluation of the Pharmaceutical tablets' chemical composition e.g. concentration of the Active Pharmaceutical Ingredient (API). In order to calibrate and asses the performance of the system for this application, different types of solid phantoms were prepared with high scattering properties that are comparable with real tablets.

6.2.1 Solid Phantom:

There are different types of phantoms according to their different applications. Applications are such as: validation of physical models and simulations, instrument performance testing and optimization, instrument calibration and testing of stability and reproducibility, inter laboratory comparison and standardization. **Epoxy resin** phantom, has essentially permanent and solid material compositions, is very suitable for routine calibration and testing of established systems. Here preparation procedure of epoxy resin phantom is discussed descriptively.

Different materials needed for preparing solid **Epoxy resin** phantom:

6.2.1.1 Epoxy Resin and Hardener:

NM 500 from **Nils Malmgren AB:** as a solvent-free epoxy.

Aliphatic Amine: as hardener which has Pot-life six hours.

The construction of **Epoxy resin** phantoms requires mixing of resin and hardener to create a transparent solid resin, which typically sets within a few days at room temperature or within a few hours at elevated temperature. The optimal procedure is to let the epoxy-harden for **12-16 h** in room temperature and then put it in an oven at **55^{o}** C for **24 h**.

Heating in oven is very important for avoiding the brittleness because without heating phantom would be hard but brittle and cannot be machined.

6.2.1.2 Scattering Particles in Phantom:

TiO_2 from **Sigma-Aldrich**

Titanium dioxide (TiO_2) powder is perhaps the most common choice as scattering particles in scientific perspective because it is produced in regular sizes, with good quality control over the size and index of refraction and it has very low absorption. The reduced scattering coefficient of the phantom increases linearly with increasing the quantity of TiO_2. TiO_2 powder resides in suspension in most media and so settles when the media is not stirred. So, it is very important to be conscious about stirring.

6.2.1.3 Absorber in Phantom:

Toner from Copying Machine

Toner from copying machine is a very good absorber in polyester because it is not bleached in epoxy, has very small scattering coefficient and remains in same form for long time. It provides nearly flat absorption spectra at 650 to1350nm wavelength region.

Schott BG36 filter crashed powder

At first Schott BG 36 filter is crashed down to powder form so that its particles size becomes lower that 1µm. As this filter has different transmission at different wavelengths in the range from 200nm to 1100nm, its powder has different absorption at different wavelength in this range. This powder was used to prepare the phantom for calibrating the system in the visible range. The transmission spectra of the Schott BG 36 filter is given below:

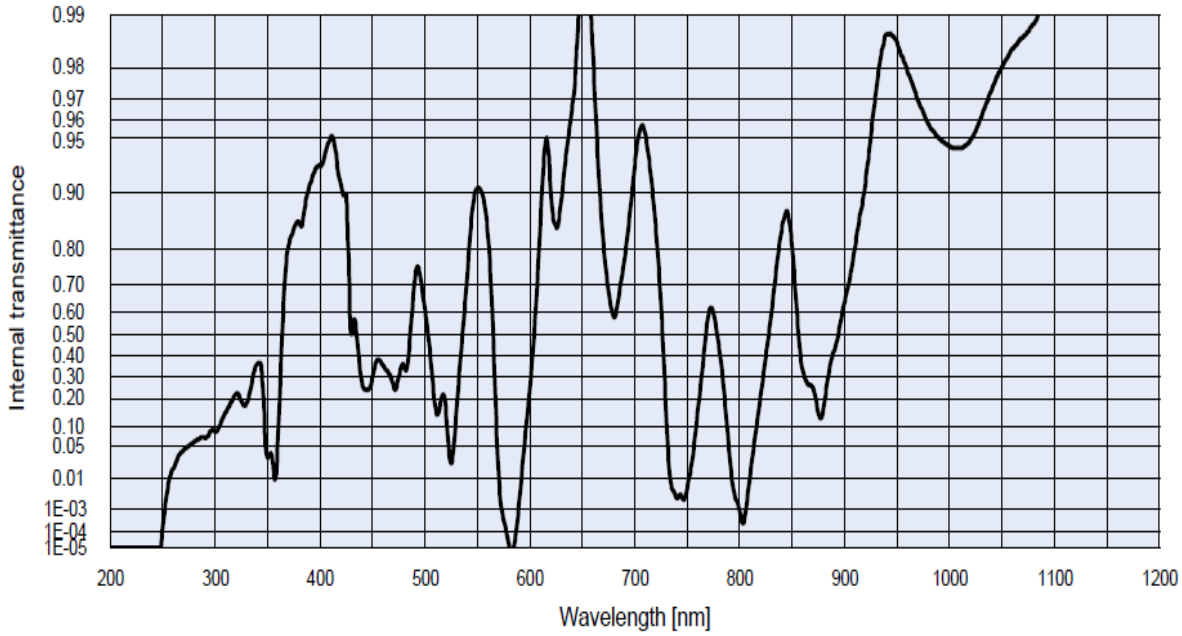

Figure 6.7: The transmission spectra of the Schott BG 36 filter [25].

In order to prepare a phantom, epoxy base and hardener should be mixed following the ratio **2.84: 1** (**epoxy: hardener**). Then different amount of **TiO_2, Bg36 filter crashed powder** and **toner (stock solution)** were mixed with epoxy & hardener to get phantoms of different optical properties.

In order to prepare the **Toner** stock solution, toner and hardener were mixed according to the ratio: **1g toner /20g hardener.** For calibration and linearity test with solid phantom, we prepared 2 set of phantoms-

1. Phantoms for **absorption series** and

2. Phantoms for **scattering series**.

6.2.2 Preparation of Epoxy phantom with high scattering and it Spectra in NIR region:

Continuous scattering and absorption spectra were recorded in the range form 950nm up to 1400 nm for epoxy phantom that was prepared with TiO_2 to mimic high scattering levels in pharmaceutical tablets. For preparing this phantom the following procedures were followed

6.2.2.1 Phantom Preparation:

1. At first, **4.77g TiO_2 and 12g of hardener** was weighed directly with 0.1 mg-accuracy and poured in a polypropylene cylindrical holder like polypropylene cup of 100ml.

2. Then the cylindrical holder was kept in ultrasonic bath for 7/8 min at room temperature. It is advantageous, since it will accelerate the pre-hardening process a little and prevent the TiO_2 from settling. At that time the mixer was not allowed to shake and the lid of the cup was put so that too much air could not dissolve in the mixture.
3. Then it was time to mix with the epoxy base, **34g** of Epoxy base was mixed with the hardener + TiO_2 Solution. Thorough mixing of the epoxy and hardener is critical to obtain a homogeneous volume that cures in a timely manner.

	Epoxy	Hardener	TiO_2
Amount	**34g**	**12 g**	**4.77g**

4. Significant heat and gas generated during this process. This mixture was stirred thoroughly and quickly with a glass stick for 10-15 minute so that larger bubbles were disappearing rather quickly. But for removing smaller bubbles, the mixture was stirred gently and slowly. About 8 - 10 minutes of stirring slowly for each phantom was fine.
5. When the mixture was stirred enough, the phantom was left for at least 12-16 hours closing the lid of the cup for removing small bubbles completely.
6. After 12-16 hours, the phantom was brought out from the cup and put in the oven setting the temperature 55^{o} C for 24 hour.

7. After baking in oven, tablets of diameter 13mm and thickness around 3mm were made from this phantom.

6.2.2.2 Measurement & Results:

At First, continuous absorption and scattering spectra of the phantom tablet were evaluated in the range form 950nm up to 1400nm with the resolution/step of 4nm. The measurements were performed in transmission mode and the optical properties of the phantom were estimated by the evaluation algorithm based on diffusion approximation model assuming refractive index=1.5. Then for precision test, the same phantom was measured at 2nd day in the range between 1100nm to 1300nm with the resolution/step of 4 nm and at 3rd day for few wavelengths in the range between 1100nm to 1300nm. The results are presented in the figure6.8 with green and red dots.

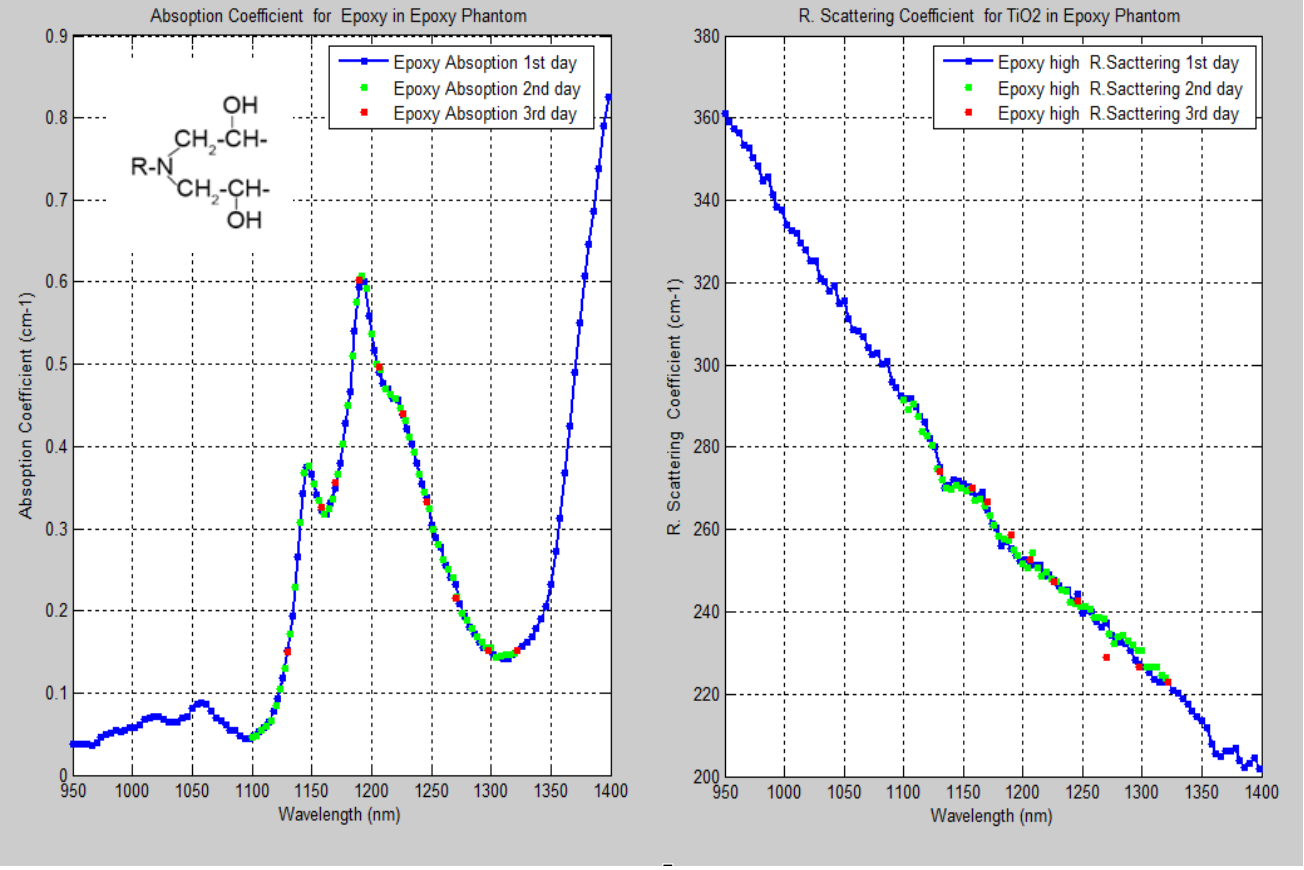

Figure6.8: scattering and absorption spectra of epoxy phantom tablet in the range form 950nm up to 1400 nm

Getting spectra with this small resolution/step (4nm) became possible only for introduction Timing Reference pulse with IRF and PTOF signal. The chemical composition of the Epoxy, CH CH2 and first OH combination, is responsible for the high absorption in the absorption spectrum (right) of phantom tablet. TiO_2 has insignificant absorption. The scattering spectrum (left) of the phantom is only for TiO_2 powder. From day to day analysis, it was found that all extracted values of optical properties for different days were just overlapping each other. This is also a good illustration for showing the precise measurement capability of the system.

6.2.3 Preparation of Phantoms for Absorber Series and Verifying Linearity of the System:

6.2.3.1 Phantom Preparation:

Five phantoms were prepared as the absorber series with same amount of scatterer and adding absorber in a step-wise manner. The following procedures were followed

1. At first, **11.5g TiO_2 and 30g of hardener** was weighed directly with 0.1 mg-accuracy and poured in a polypropylene cylindrical holder.
2. Then the cylindrical holder kept in ultrasonic bath for 7/8 min at room temperature.
3. Then, **85g** of Epoxy base was mixed with the hardener + TiO_2 Solution and was stirred quickly to get homogeneous volume within a short time.
4. This homogeneous mixture was divided into five equal quantities by weighting with 0.1 mg-accuracy scales and then each quantity was poured into a 100 ml polypropylene cup.

5. Then each polypropylene cup was labeled and Toner stock solution was added in cups with increment of 0.088g from zero to 0.36 g. Preparation table is as follows:

Phantom No.	Epoxy in g	Hardener in g	TiO_2 in g	Stock solution in g	Toner weight percentage %
Phantom **1**	17	6	2.3	0	0
Phantom **2**	17	6	2.3	(0.088)	0.0165
Phantom **3**	17	6	2.3	(0.180)	0.036
Phantom **4**	17	6	2.3	(0.273)	0.0508
Phantom **5**	17	6	2.3	(0.360)	0.0667
Total amount	**85**	**30**	**11.5**		

6. Now each mixture was stirred moderately for first 10-15 minutes and then stirred slowly for about 8-10 minutes with a glass stick for removing big and smaller bubbles respectively.
7. Then the phantoms were left for at least 12-16 hours closing the lids of the cups. After 12-16 hours, the phantoms were brought out from the cup and put in the oven setting the temperature 55^{o} C for 24 hour. After baking, a tablet of diameter 13mm and of thickness around 3mm was made from each phantom.

6.2.3.2 Measurement & Results:

Five tablets from five phantoms of absorber series were measured with PTOF system at six wavelengths in transmission mode and the wavelengths are as follows: 1158nm, 1190nm, 1206nm, 1226nm, 1246nm and 1270nm. Then optical properties were estimated using the evaluation algorithm based on diffusion approximation model assuming refractive index=1.5.

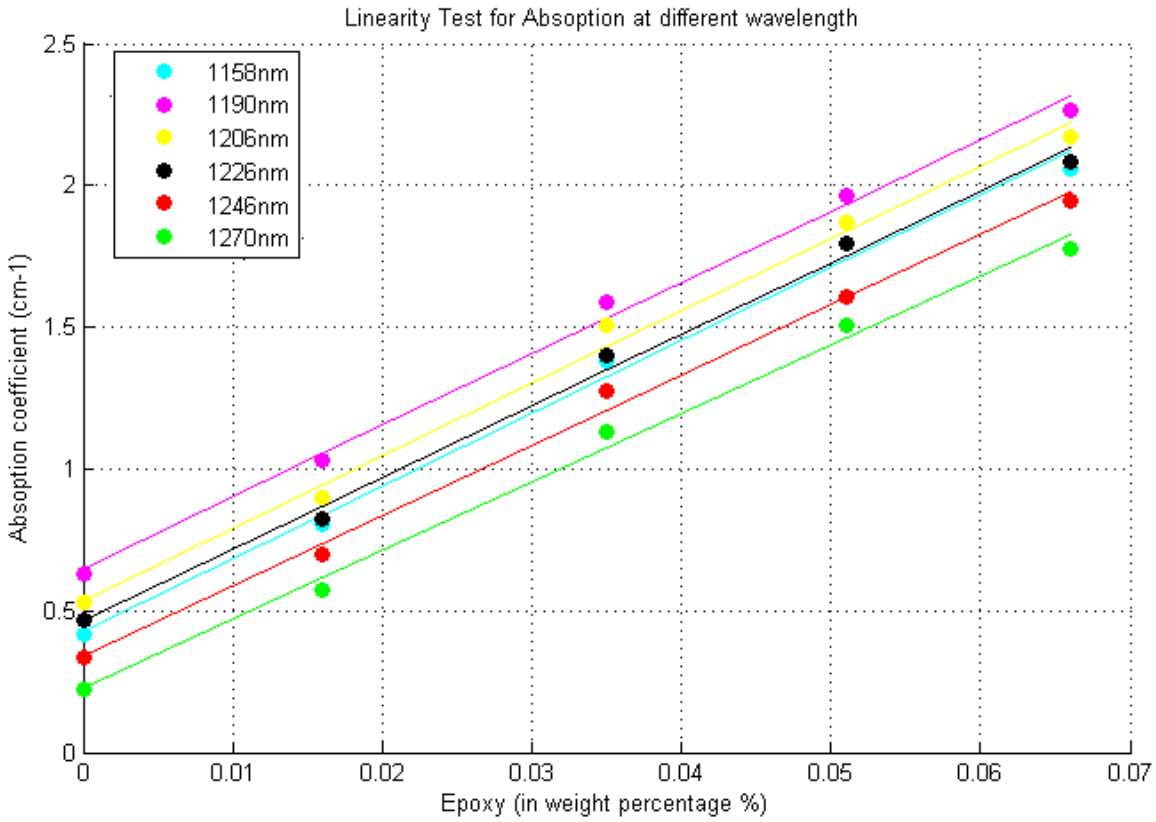

Figure6.9: Linearity of absorption μ_a for Toner at different wavelengths.

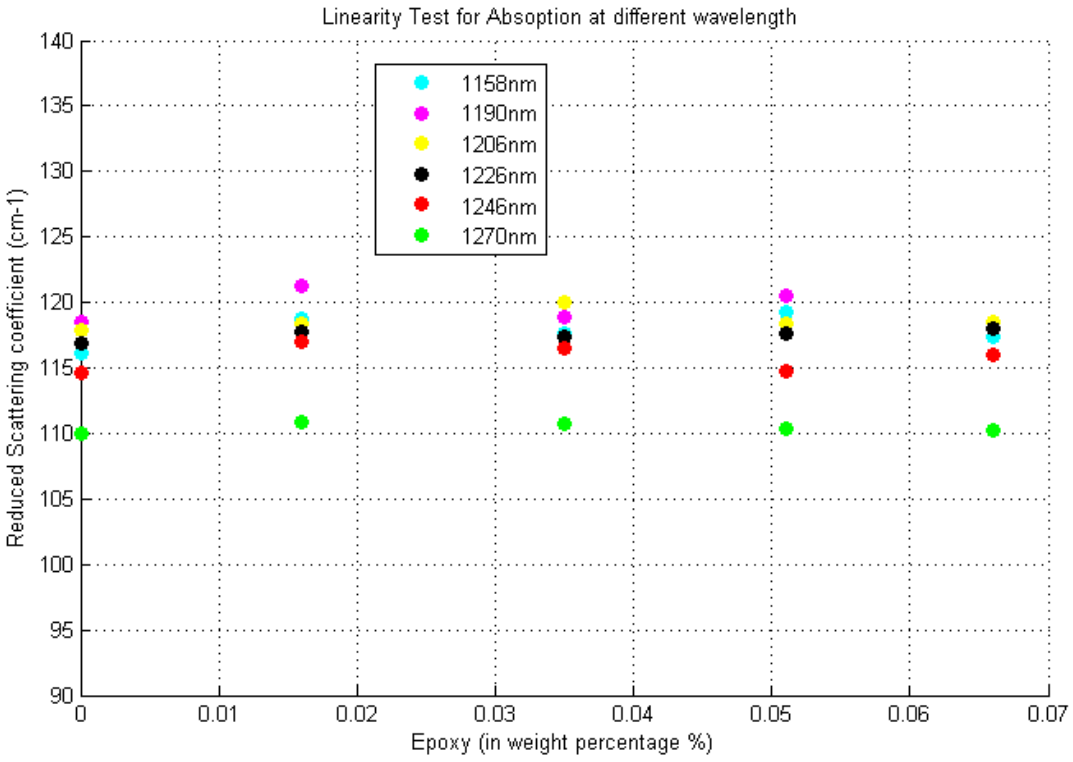

Figure6.10: Linearity of absorption (μ_a) for Toner at different wavelengths.

At these six wavelengths epoxy itself has high absorptions (Form Figure6.4) and each phantom has exactly the same amount of epoxy. Moreover, the amounts of added Toner (stock solution) are insignificant for changing the weight percentage of the epoxy. So, the different absorptions of the tablets, made for absorber series phantoms, are only for adding different amounts of Toner (stock solution).

Counting the weight percentage of the Tone (stock solution), it is found that at all wavelengths with increasing the weight percentage of the Tone the absorption coefficient (μ_a) is increasing very linearly and reduced scattering coefficient (μ_s') remains constant. This is how; verification of **linearity in absorption measurement** was done.

6.2.4 Preparation of Phantoms for Scatterer Series and Verifying Linearity of the System:

6.2.4.1 Phantom preparation:

In order to verify the linearity in scattering measurements, another set of five solid phantoms were prepared as scatterer series with same amount of absorber and adding scatterer in a step-wise manner. The following procedures were followed

1. At first, **2.35g TiO_2 and 15g of hardener** was weighed directly with 0.1 mg-accuracy and poured in a polypropylene cylindrical holder.
2. Then the cylindrical holder kept in ultrasonic bath for 7/8 min at room temperature.
3. Then, **42.64g** of Epoxy base was mixed with the hardener + TiO_2 Solution and was stirred quickly to get homogeneous volume within a short time. .
4. This homogeneous mixture was divided into five equal quantities by weighting with 0.1 mg-accuracy scales and then each quantity was poured into a 100 ml polypropylene cup.
5. Then each polypropylene cup was labeled and phantoms of increasing scatterer series were prepared by adding TiO_2 again in cups from 0.94g to 4.7g with increment of 0.47g. Preparation table is as follows:

	Epoxy in g	Hardener in g	TiO_2 (1^{st} time) in g	TiO_2 (2^{nd} time) in g	TiO_2 weight percentage %	Epoxy weight percentage %
Phantom **6**	8.524	3	0.47	.94	7.54	68.4
Phantom **7**	8.524	3	0.47	1.88	14.1	63.6
Phantom **8**	8.524	3	0.47	2.82	19.7	59.4
Phantom **9**	8.524	3	0.47	3.76	24.6	55.8
Phantom **10**	8.524	3	0.47	4.7	29	52.6
Total amount	**42.68**	**15**	**2.35**			

6. Now each mixture was stirred moderately for first 10-15 minutes and then stirred slowly for about 8-10 minutes with a glass stick for removing big and smaller bubbles respectively.
7. Then the phantoms were left for at least 12-16 hours closing the lid of the cups. After 12-16 hours, the phantoms were brought out from the cup and put in the oven setting temperature 55^{o} C for 24 hour. After baking, a tablet of diameter 13mm and of thickness around 3mm was made from each phantom.

6.2.4.2 Measurement & Results:

The Data acquisitions for these tablets were performed with the system in transmission mode at six different wavelengths in NIR region and optical properties were estimated using the evaluation algorithm based on diffusion approximation model assuming refractive index=1.5.

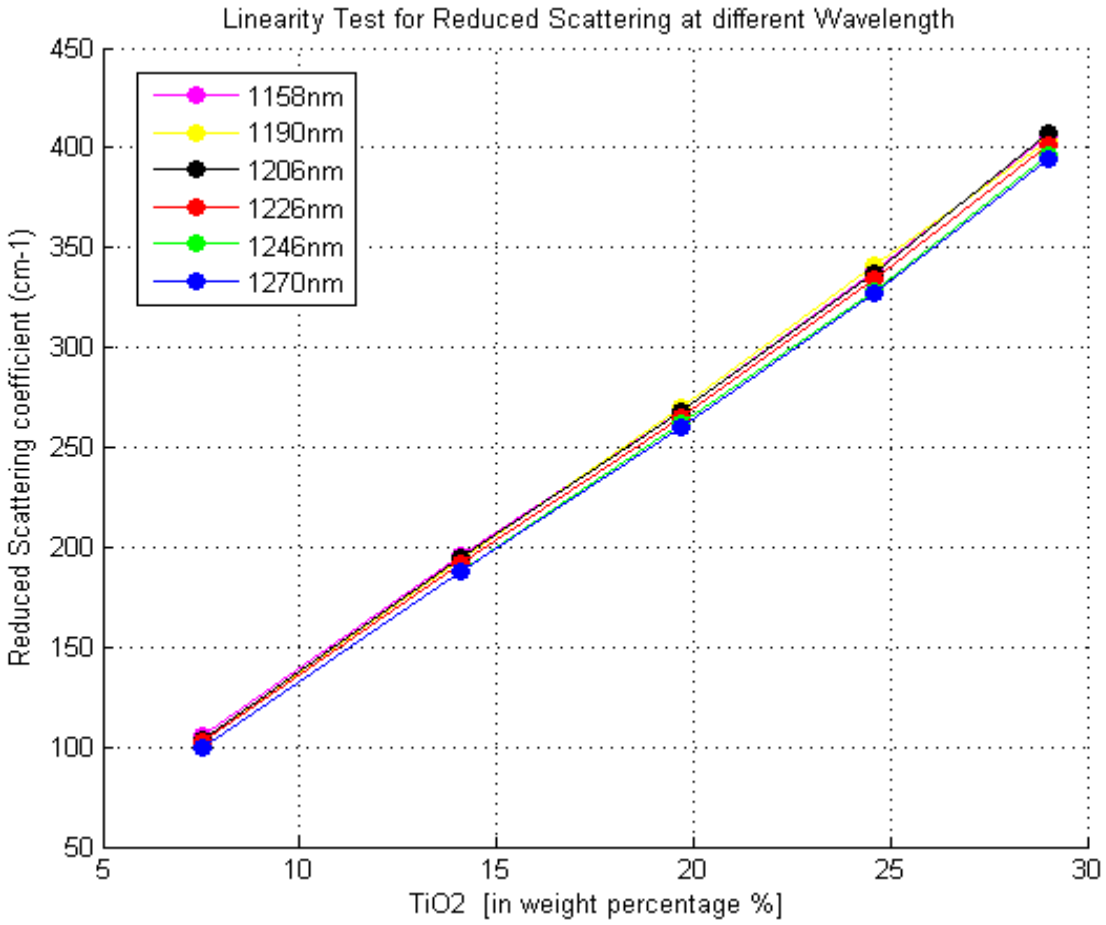

Figure6.11: Linearity of Reduced scattering ($\mu_{s'}$) for TiO_2 at different wavelengths.

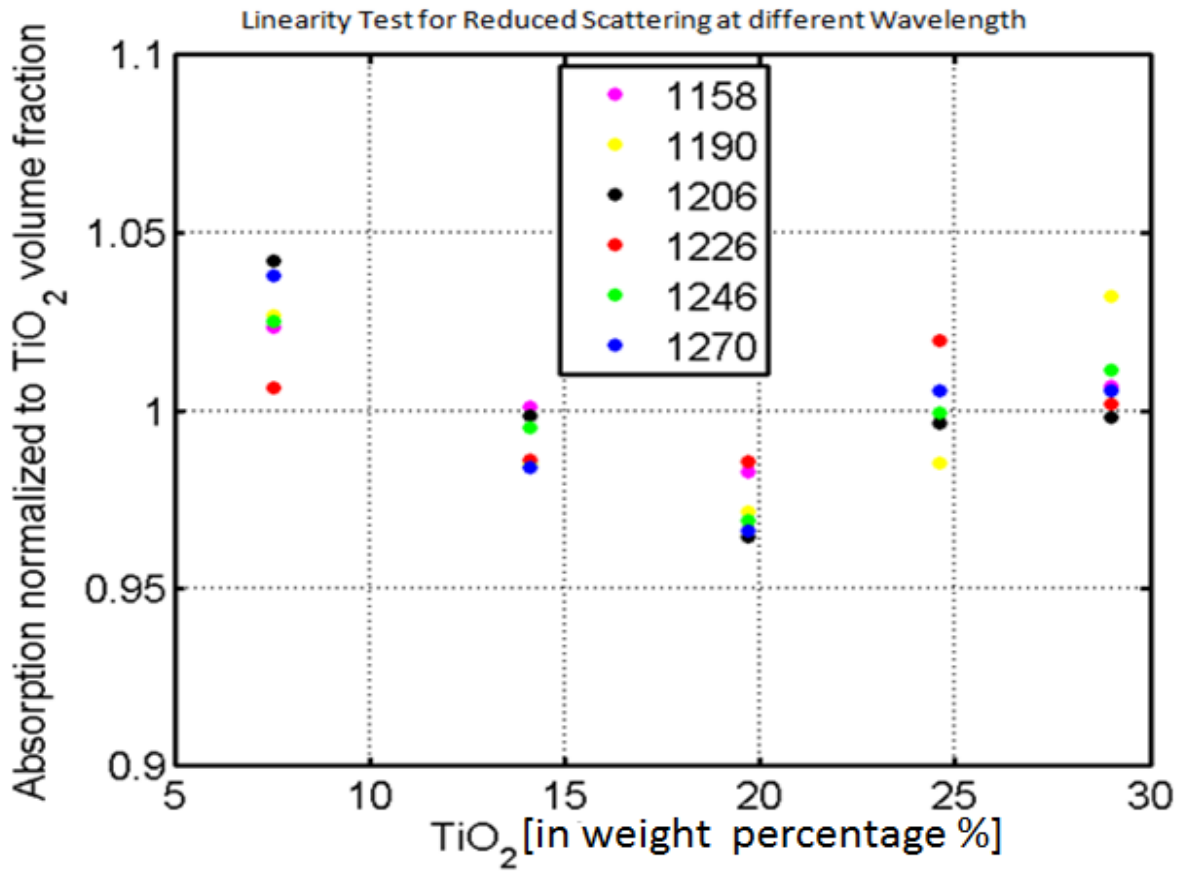

Figure6.12: Linearity of Reduced scattering ($\mu_{s'}$) for TiO_2 at different wavelengths.

Here, no extra absorber was used because epoxy itself has very high absorption at the NIR region. TiO_2 was added in five phantoms of scatterer series in a step-wise manner and the amounts of TiO_2 in phantoms were quite significant. That's why, with increasing the amount of TiO_2 in phantoms, the weight percentage of TiO_2 increases while the weight percentage of epoxy decreases. Counting these changes of the weight percentage of epoxy and TiO_2, it was observed that for increasing the weight percentages of the TiO_2 the reduced scattering increased very linearly while absorption coefficient decreased slightly. After, normalizing the absorption coefficient values it was found that they were quite consistent. The small variation in absorption of five tablets is due to the non-homogeneity and small gradient of the TiO_2 particles density in five phantoms.

6.4.5 Some Important Issues about Preparing Epoxy Phantom:

Following the above mentioned procedure properly, we were able to prepare and measure the phantoms of required optical properties. During the experiments, it is important to be conscious about not to form gas bubbles in the phantoms. Gas bubbles may be formed as a result of putting the mixture in the oven too early and for keeping the lid of the hardener cup open and for very quick stirring. At the time of ultrasonic bath, there was possibility for gaining high temperature and so water of the ultrasonic bath was changed several times. If the temperature of the hardener increases, it will make quick reaction with the epoxy base and the gas bubbles will not get enough time to escape from the mixture.

It is to be noted that the optical properties of phantoms made by using the same procedure may give different result for different supply of ingredients. One reason is that the particle size of TiO_2 may vary from old supply to new supply and the scattering of light depends on particle size. As a result, there is a chance to get different reduced scattering coefficient μ'_s, using the same amount.

In case, if very old hard Epoxy base is needed to use, it should be warmed up gently until it gets back to its natural form (honey like form). Then it should be left for cooling. Because, after mixing this lukewarm epoxy base with hardener, it will never be possible to remove bubbles completely from phantom.

At the time of handling epoxy and hardener, it is very important to use gloves for protection. A very nasty allergy can easily be occurred on skin for contacting it with skin. Using Acetone or any other solvent is strictly forbidden to clean epoxy that got on hands. It might as well inject the epoxy directly into veins.

6.2.5 Verification the Stability of the System with Tablets Same Ingredients but with Different Thickness:

In order to verify the system, another experiment was done. Here, five tablets were prepared from the same phantom slab with same diameter but with different thicknesses. Ideally, for uniformly homogenous medium, optical properties should not be changed with the thickness of the medium. This phantom was prepared following the same procedures mentioned before (section 6.2.2) with ingredients mentioned below.

	Epoxy	Hardener	TiO_2
Amount	**34g**	**12 g**	**2.39g**

The idea behind the experiment was to find effects on measurement of the system for changing the thickness of the tablet slab. Here, all tablets were taken from the same phantom slab because big phantom may have small gradient in scattering particles density and our expectation is to get exactly same optical properties for all tablets. Then these tablets were measured with the system in transmission mode at six wavelengths and results were estimated using the evaluation algorithm based on diffusion approximation model assuming refractive index=1.5. The results are as follows:

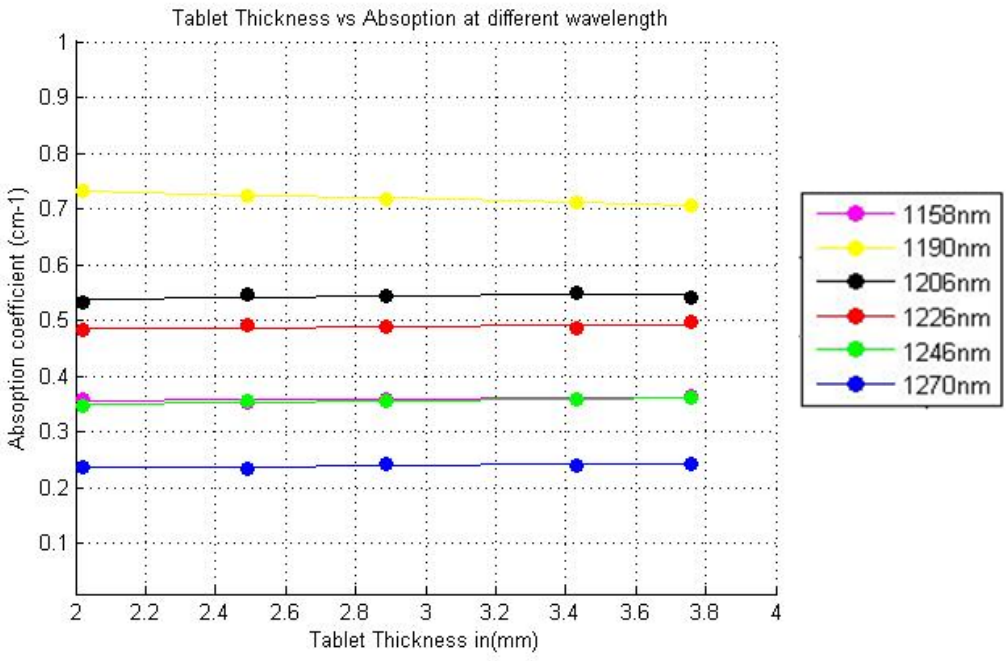

Figure6.13: Tablet thickness vs. absorption coefficient at different wavelengths

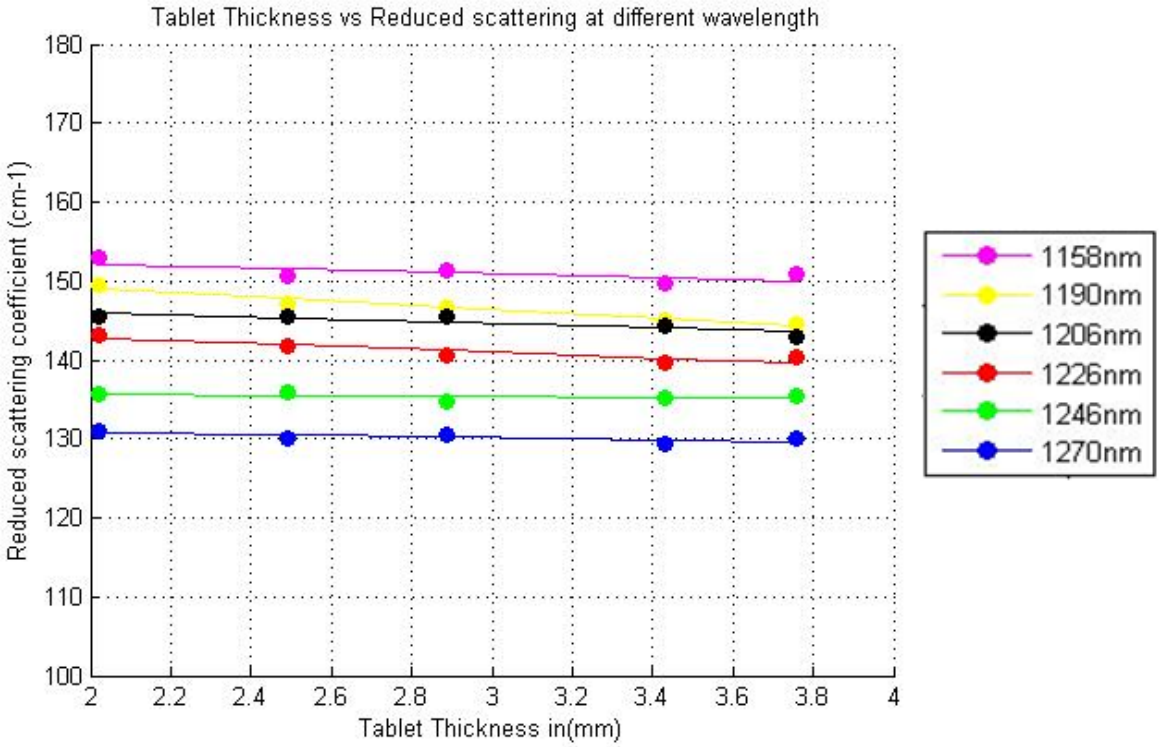

Figure6.14: Tablet thickness vs. reduced scattering at different wavelengths

From the figures, it is verified that there is no effect on measurement of the system due to changes of the thickness of the same sample. System is capable of provide correct results regardless of thickness.

6.3 Verification of the Consistency of the Experimental Data along with Theoretical Model:

For good performance of the system, it is very important to verify the consistency of the experimental data along with theoretical model. In order to confirm their consistency, different results were verified which were obtained by fitting the experimental data with theoretical model using different fit ranges. Two phantoms- one with high absorption and another with low absorption were measured and experimental data were fitted with Monte Carlo model using different fit ranges from 10% to 80% to get optical properties. All fitting range result nearly the same absorption & reduced scattering coefficients for each phantom.

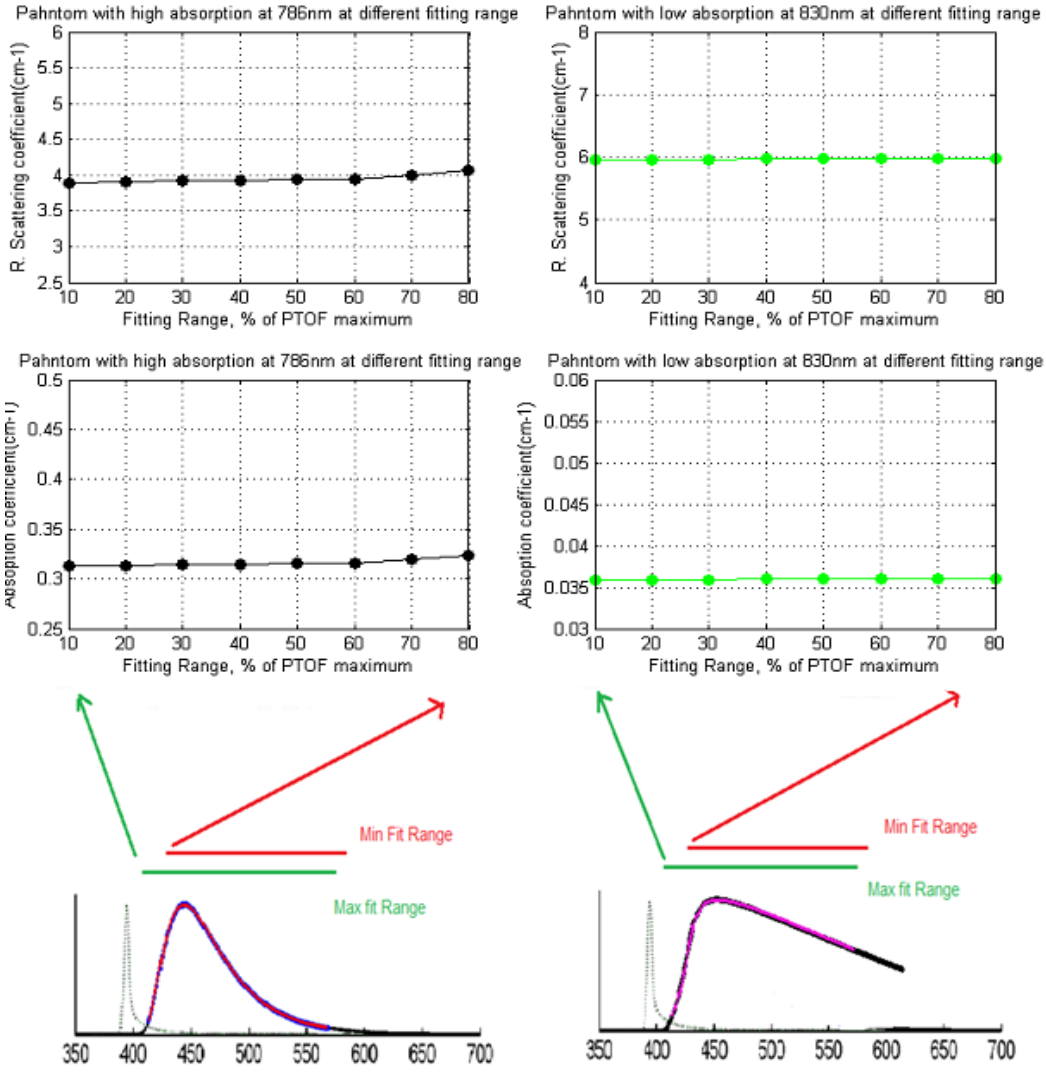

Figure6.15: verification of the results with different fit ranges

This is how; verification of the consistency of the experimental data along with theoretical model was performed successfully.

Chapter 7

7 BG36:TiO_2 Epoxy Phantom & Limited Resolution Effects of the System:

In order to calibrate PTOF system in the range from 650nm to 1050nm, new type of epoxy resin based phantoms was prepared with titanium dioxide and crashed powder of BG36 color filter with the aim to get very high reduced scattering and remarkably different absorption at different wavelengths like real pharmaceutical tablets.

7.1 Phantom Preparation:

BG36 color filter has very interesting absorption spectrum (figure 6.7) in the range from 650nm to 1050nm. In order to prepare this calibration phantom, we followed the same procedures which were used for making epoxy phantom with toner. But here instead of toner stock solution, crashed powder of BG36 filter was used following the quantity.

	Epoxy	Hardener	TiO_2	crashed powder of BG36 filter
Amount	**34.0129 g**	**11.988 g**	**6.04g**	**2.333**

At first TiO_2, crashed powder of BG36 color filter and hardener were weighed according to the tabulated values with 0.1 mg-accuracy and then they were put together in ultrasonic bath for 7/8 min using polypropylene cylindrical holder at room temperature. Then, Epoxy base was mixed with the hardener+ crashed powder of BG36 + TiO_2 Solution and the mixture was stirred gently for at least 20 min to get homogeneous volume. After complete preparation of phantom, tablets of diameter 13mm and of thickness around 3mm were made from the phantom.

7.2 Limited Resolution Effects on μ_s' and μ_a:

After preparing the system capable to produce very accurate and precise results, continuous absorption & scattering spectra of the calibration phantom were recorded in the range from 650 to 1050 nm with the resolution/step of 2nm. The optical properties were estimated using the evaluation algorithm based on diffusion approximation model assuming refractive index=1.5. Figure7.1 showed the measured absorption and reduced scattering spectra of the tablet prepared from the BG36 phantom.

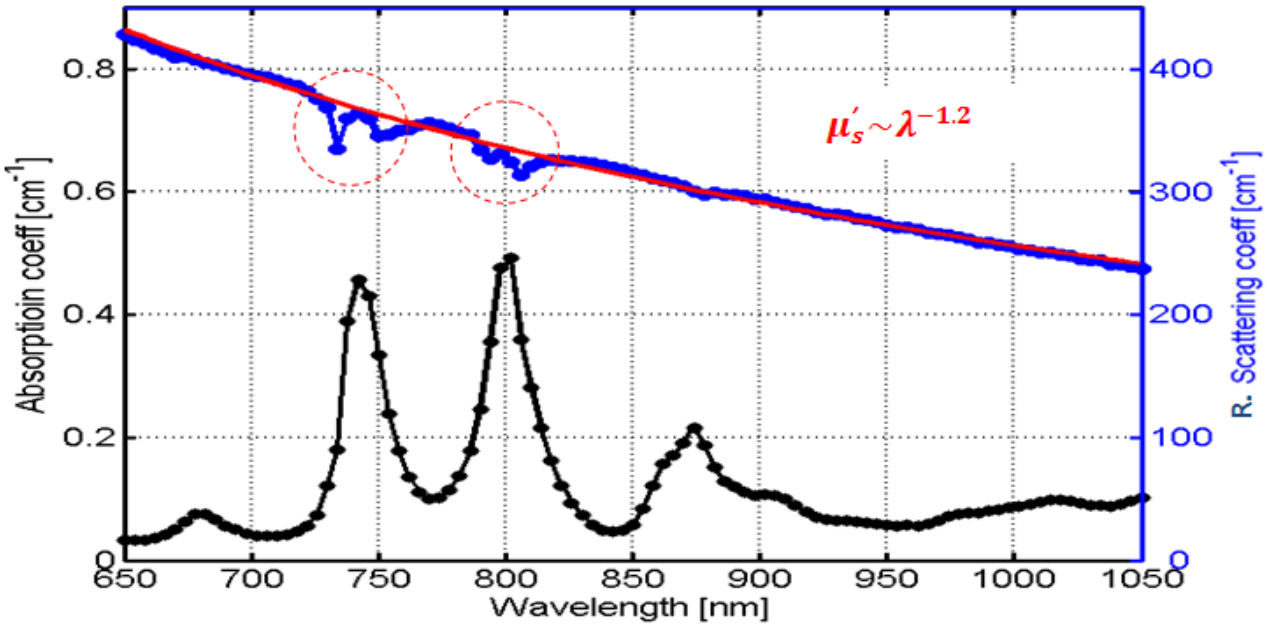

Figure7.1: Spectra of the BG36:TiO_2 epoxy phantom

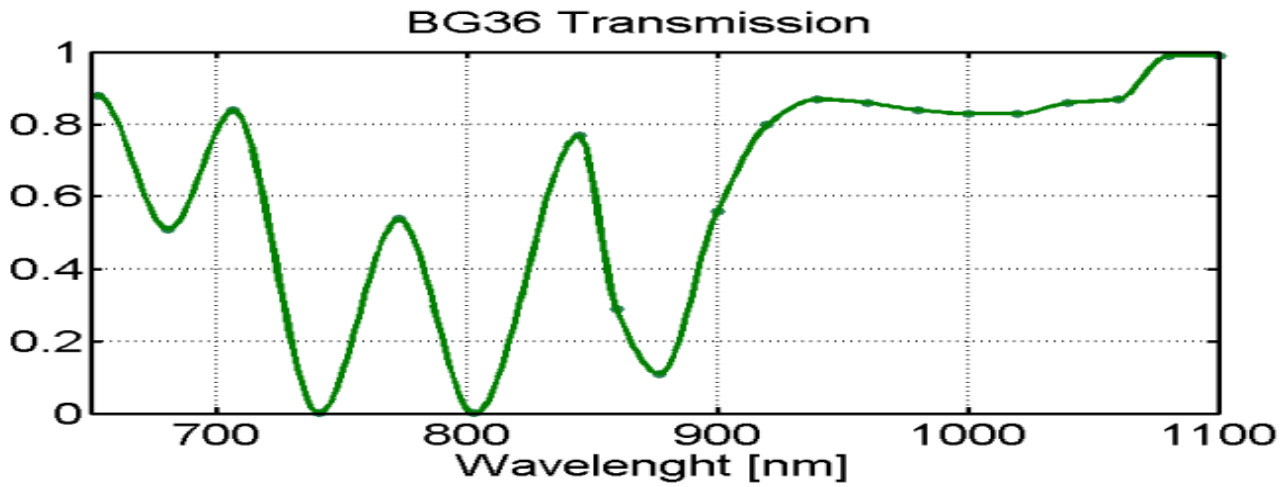

Figure7.2: Transmission spectra of the BG36 Filter [24].

Absorption (figure7.1) spectrum of the phantom determined by PTOF is exactly similar to the absorption spectra of the Bg36 glass filter (figure7.2). By doing linear curve fitting of reduced scattering coefficients (μ_s') values, it was found that reduced scattering coefficient (μ_s') decreases linearly with increasing the wavelength, which follows scattering coefficient (μ_s')$\sim [\text{wavelength}(\lambda)]^{-1.2}$, except for those wavelengths which are very close to the wavelength of peaks absorption. At those wavelengths residual mistakes in determination of the absorption and scattering coefficients occurred for source resolution and dispersion in probe pulse.

AOTF provides pluses with spectral width of 3-6nm for 650nm to 1100nm region and 6-12nm for 1100nm to 1850nm region [10]. For the spectral width of probe pulse in time domain, the shape of the detected pulse is changed undesirably in the time domain due to remarkable attenuation at singular wavelength where absorption is maximum. When any probe pulse of desired wavelength, which is very close to wavelength of peak absorption of sample, is sent to a sample, the attenuation of the intensity profile of the (spectrally) broadened pulse at the peak absorption wavelength becomes much stronger than that at desired wavelength. This phenomenon creates two effects. Firstly, the peak position (considering intensity profile) of the detected pulse is changed in time domain. Secondly, the transmittance curve (PTOF signal) for sample cannot be recorded for desired wavelength from measurements. The transmittance curve, which is found, is rather averaged over the spectral bandwidth of the pulse. The changing of the peak position (considering intensity profile) of the detected pulse provides extra temporal drifts in sample measurements. The peak position of the sample measurement pulse can be shifted forward or backward direction comparing to the IRF peak position. When the mutual shift between IRF and sample pulse is negative ($\Delta\tau < 0$), μ_s' is underestimated and if the mutual shift is positive ($\Delta\tau > 0$), μ_s' becomes overestimated. The accurate estimation and control of these extra temporal drifts are nearly impossible. This is how; the measurement at wavelengths, which are close to peak absorption wavelength, are affected and causes residual errors in determination of the absorption and scattering coefficients.

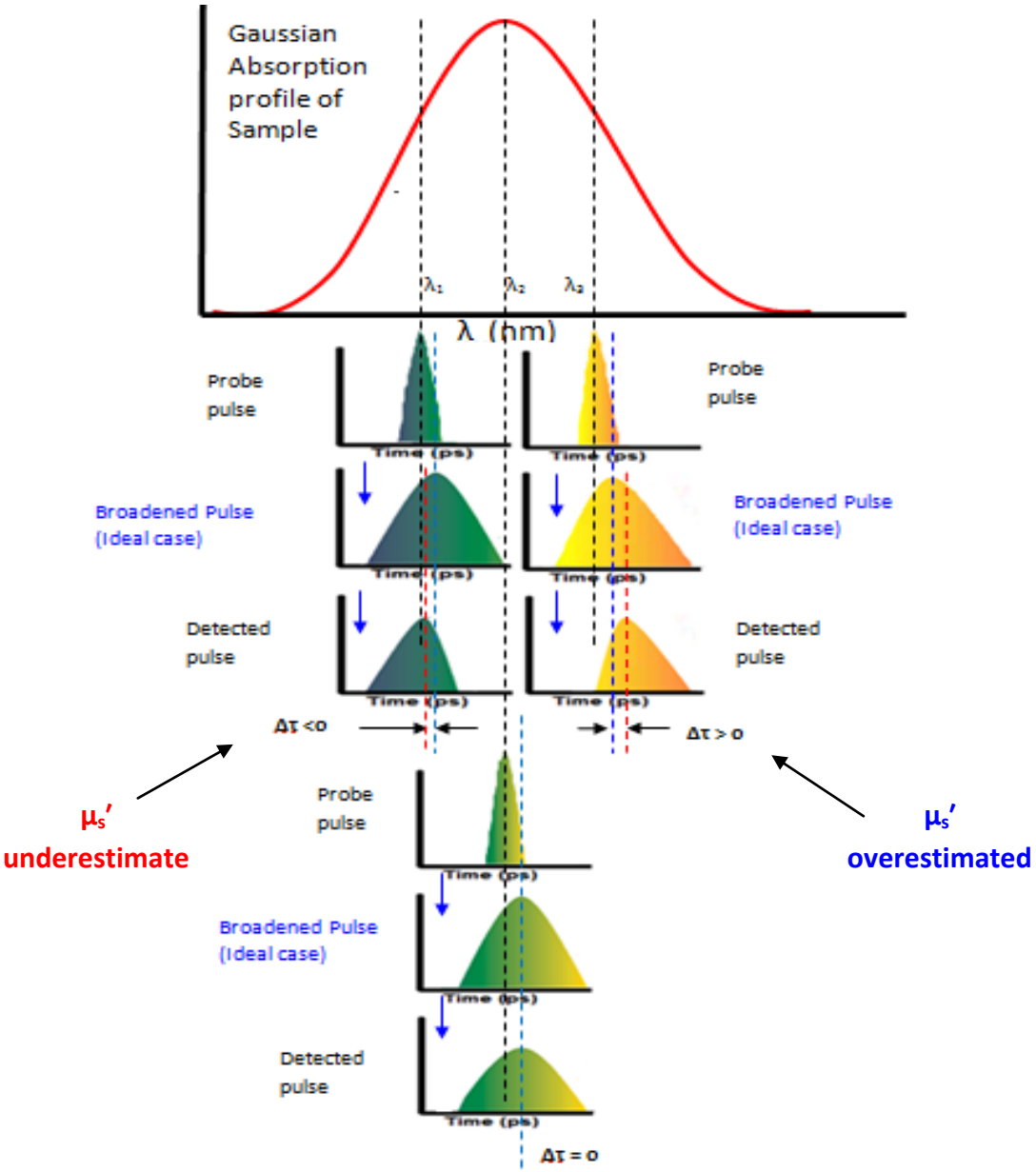

Figure7.5: Showing how the shape of the probe pulse changes for Gaussian absorption profile of the sample due to dispersion in the probe pulse and change the peak position of the pulse in time domain. Colors represent only for illustration of dispersion.

In order to illustrate the second effect and the reason for occurring residual errors, diffuse transmittance curves of test data (averaged over the spectral bandwidth of sample) are fitted with modeled diffuse transmittance curves.

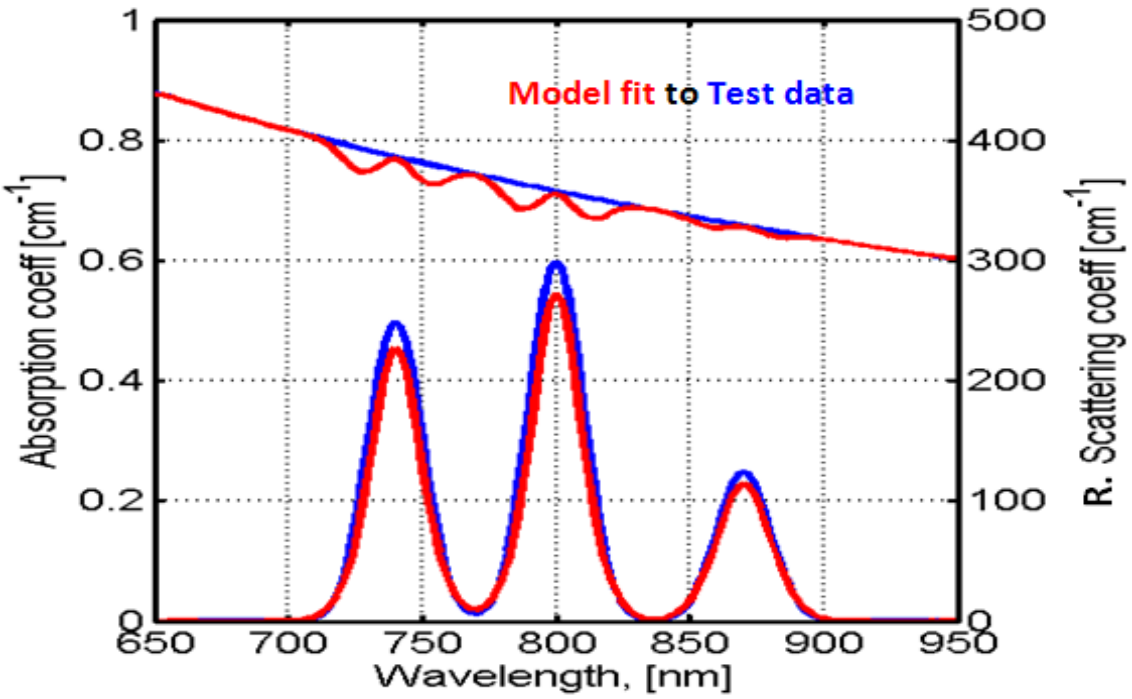

Figure 7.6: Deviation in spectra for fitting the transmittance curves of test data with modeled transmittance curves

The diffuse transmittance curve for sample (turbid material) is a function of its absorption (μ_a) and reduced scattering coefficient (μ_s') coefficient which are wavelength dependent. For modeling the experiment let us consider, linearity of reduced scattering coefficients (μ_s') with wavelengths is represented by blue straight line and absorption coefficient (μ_a) values are represented by blue Gaussian profile. Then for each wavelength, the diffuse transmittance $[T_1(\mu_a(\lambda), \mu_s'(\lambda))]$ curve is modeled with corresponding μ_s' & μ_a values.

Then each modeled diffuse transmittance curve is averaged over the spectral width of pulse for each probe wavelength.

$$T_2(\mu_a(\lambda), \mu_s'(\lambda)) = \int_{\lambda_{min}}^{\lambda_{max}} T_1(\mu_a(\lambda), \mu_s'(\lambda))$$

Then, each averaged transmittance $[T_2(\mu_a(\lambda), \mu_s'(\lambda))]$ curve for probe wavelength is fitted with modeled diffuse transmission curve $[T_1(\mu_a(\lambda), \mu_s'(\lambda))]$ and new values of μ_a & μ_s' are obtained. These new scattering and absorption coefficient are plotted with red points (red lines and curve) for different wavelengths and it is found that these new spectra have similar nature with continuous absorption & scattering spectra of BG-36 phantom.

Chapter 8

8 Experiments Leading towards Pharmaceutical Industry:

8.1 Pharmaceutical Tablets Preparation:

One of the target applications of PTOF system is to precisely determine drug concentration (API) in a pharmaceutical tablet. In practice the tablets are fabricated not simply from powders but from small granules composed from the drug and other components like MCC, lactose in order to make drug distribution in the tablet more uniform. However, the drug absorption is a tiny fraction of the absorption of other components like MCC and lactose and overall scattering property of the tablet is very high. With conventional NIR spectroscopy, measurements of tablet adsorption or more precisely tablet extinction spectra are severely affected by the scattering.

In our pilot experiment for measuring Active Pharmaceutical Ingredient (API) of the pharmaceutical table, six sets of tablets were prepared with six different granulates naming 1, 5, 11, 13, 17 and 19 from Astra Zeneca. Each set has three subsets according to three different sieve sizes: below 150 µm, between 150 µm – 400 µm and greater 400 µm. Each subset has 3 tablets of same amount of ingredients [13]. So, as a whole total 54 tablets were prepared for whole experiment procedure.

8.2 Absorption & Scattering Spectra for 4 tablets:

As a first step, full scattering and absorption spectra of four tablets, e.g., two tablets from granulates 1 and two tablets from granulates 19 with sieve sizes less than 150 µm and greater than 400 µm, were recorded in order to get two maximum differences in scattering spectra and two maximum differences in absorption spectra. Both granulates have different drug concentrations of API, as shown in the table mentioned above.

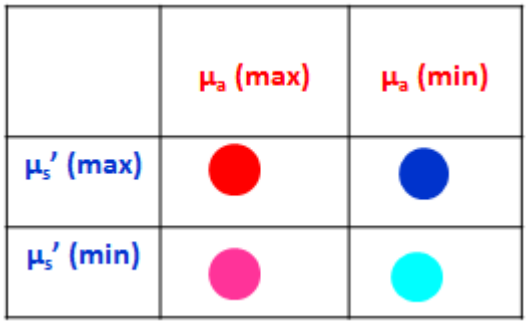

Figure8.1 Tablets for first experiment

The measurements were performed from 950 to 1350 nm at NIR region with the resolution/step of 4 nm. Figure8.2 & 8.3 are showing the results of absorption and scattering coefficients of four selected tablets evaluated using data evaluation algorithm based on Diffusion approximation model assuming refractive index 1.5.

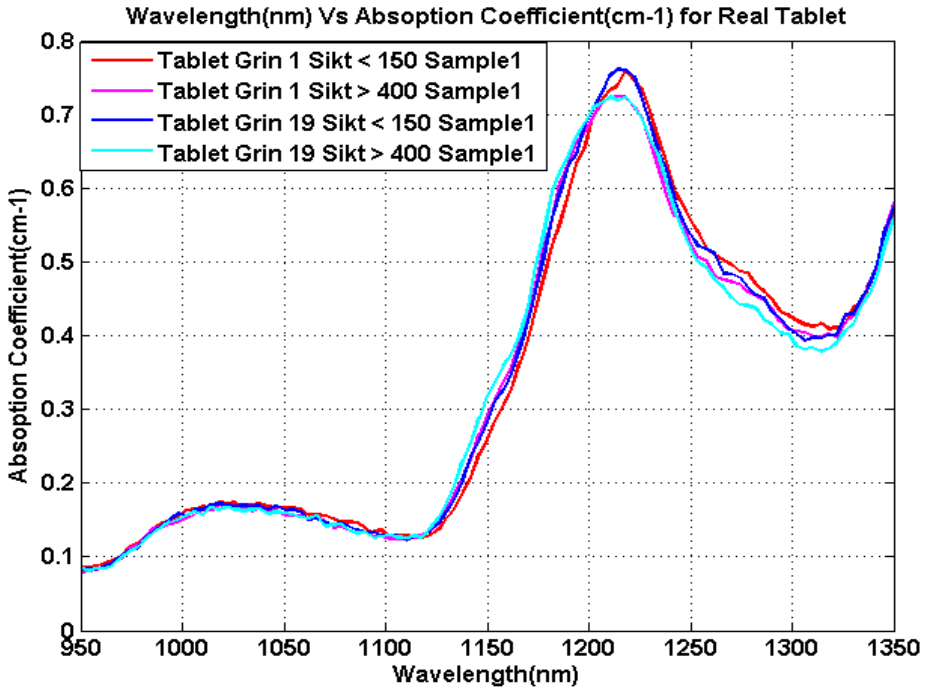

Figure8.2: Absorption spectra of four Pharmaceutical Tablets

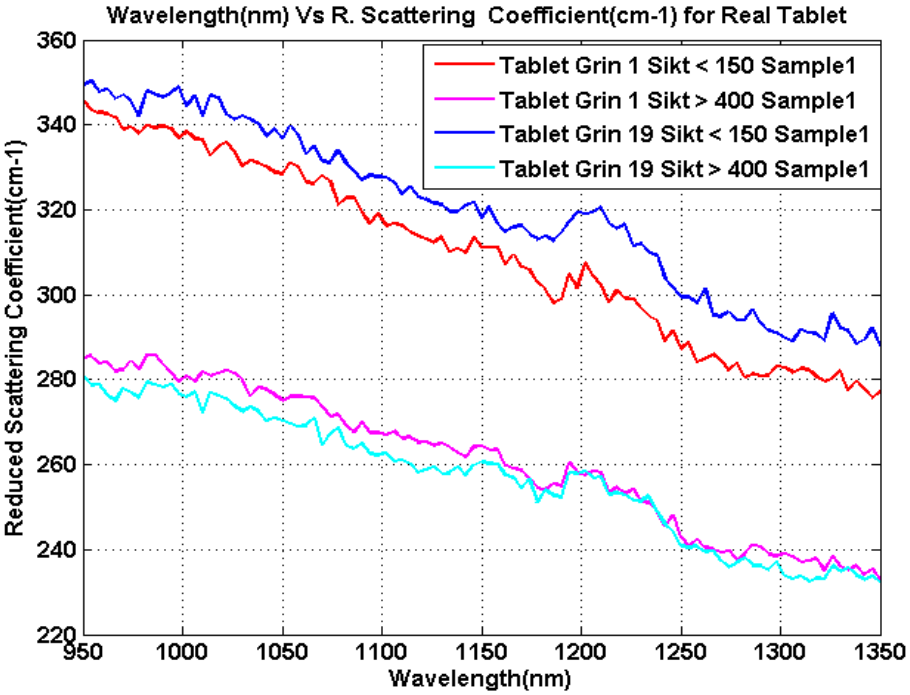

Figure8.3: Reduced Scattering spectra of four Pharmaceutical Tablets

In the result, the differences in scattering spectra are according to our expectation while the differences in absorption spectra are really not following what we expect. Absorption spectra differences are larger for different sieves than for different API (drug) concentrations. However, these are the first spectra of pharmaceuticals tablet in such a bandwidth. We are guessing there were some problems in tablets preparation with proper contents

Then the spectra of 54 tablets were measured.

The following figure represents the normalized extinction spectra for 54 pharmaceuticals tablets and these extinction spectra were measured from Astra Zeneca using NIR spectroscopy.

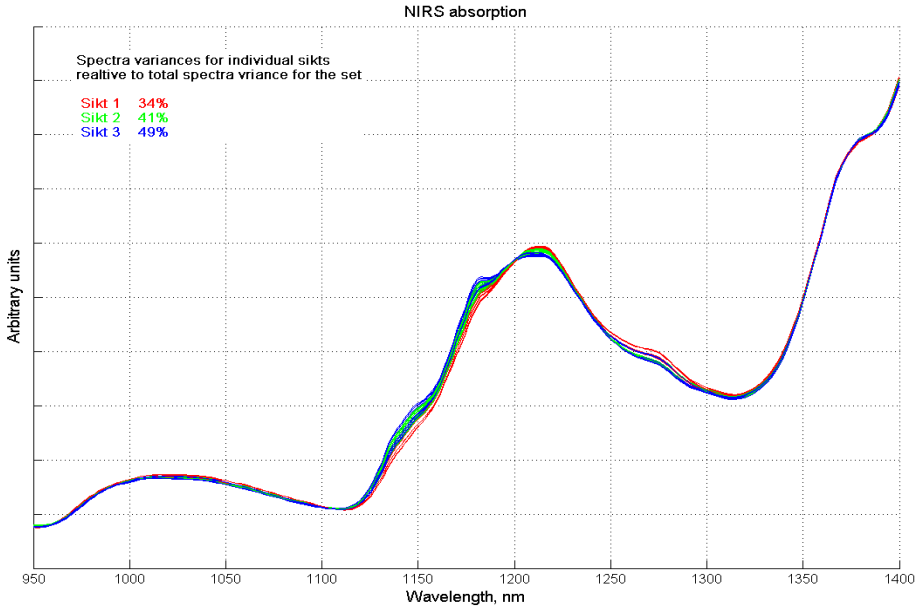

Figure8.4: Normalized NIR extinction spectra from Astra Zeneca [13].

The extinction spectrum of actual drug is shown with extinction spectrum of tablet.

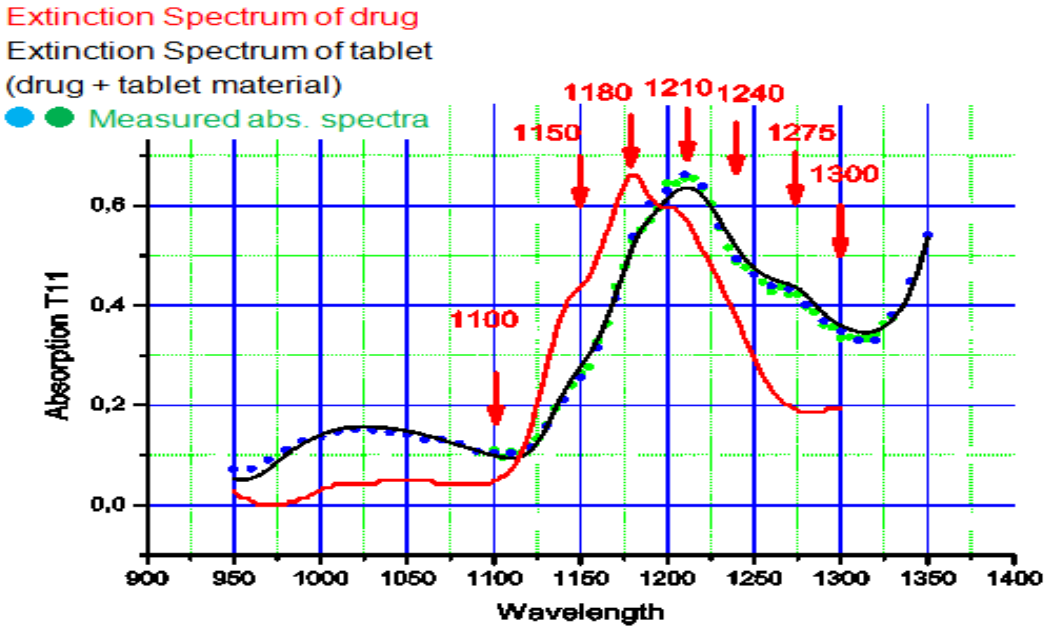

Figure8.5: Selected wavelength for measurement [13].

Actual API extinction spectrum is quite weak comparing the spectrum of the tablet. How, API extinction spectrum is normalized here in order to select useful wavelengths for estimating the API content in tablet. Those wavelengths were selected for spectrum of each tablet where the variation is high between API and tablet spectra [13]. 54 tablets were measured with TFOT system in transmission mode for wavelength 1030nm, 1115nm, 1150nm, 1180nm, 1210nm, 1240nm, 1275nm & 1310nm. Then, the absorption and scattering coefficients were extracted using data evaluation algorithm based on Diffusion approximation model assuming refractive index 1.5.

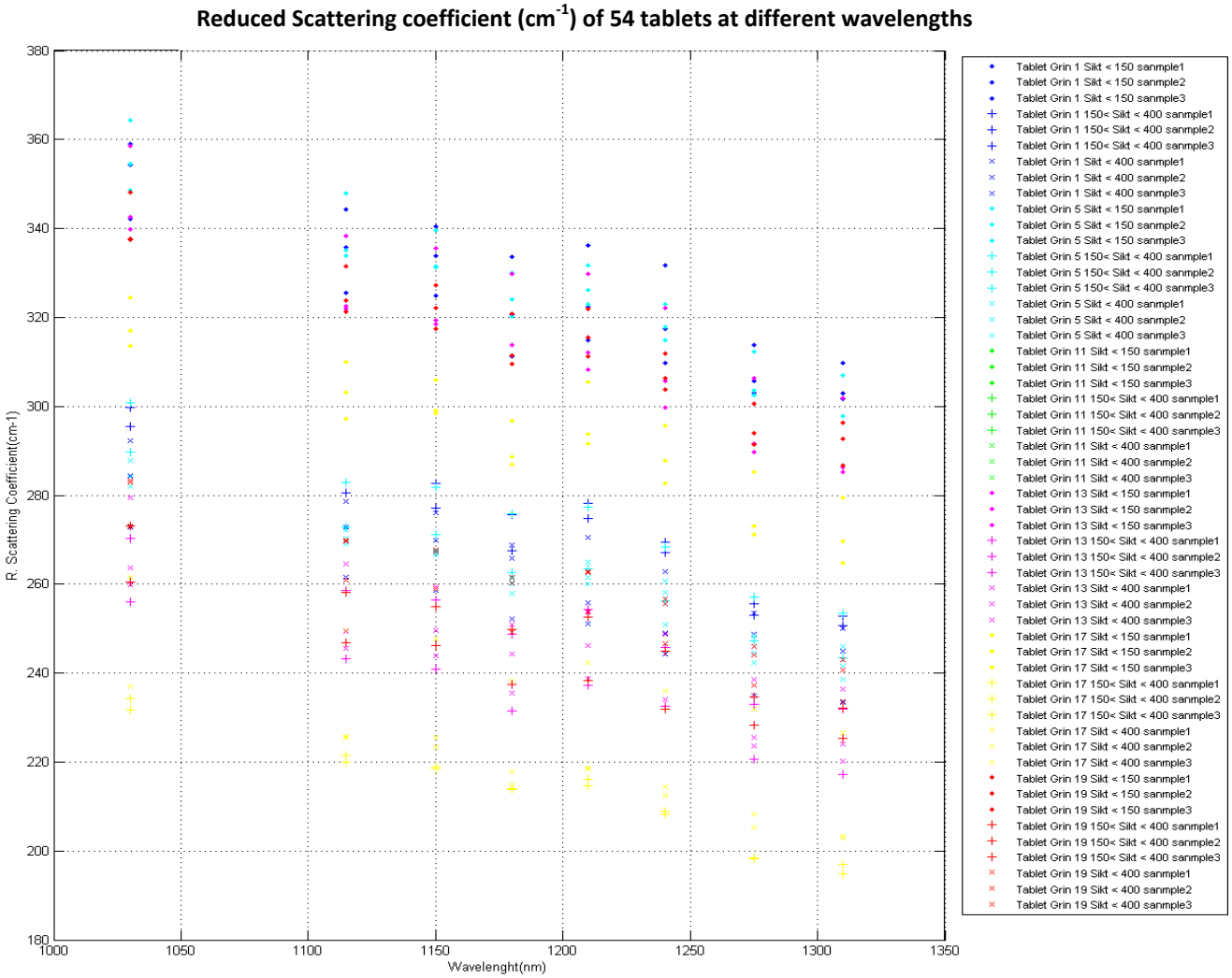

Figure8.6: Reduced Scattering coefficient (cm^{-1}) of 54 tablets at eight selective wavelengths.

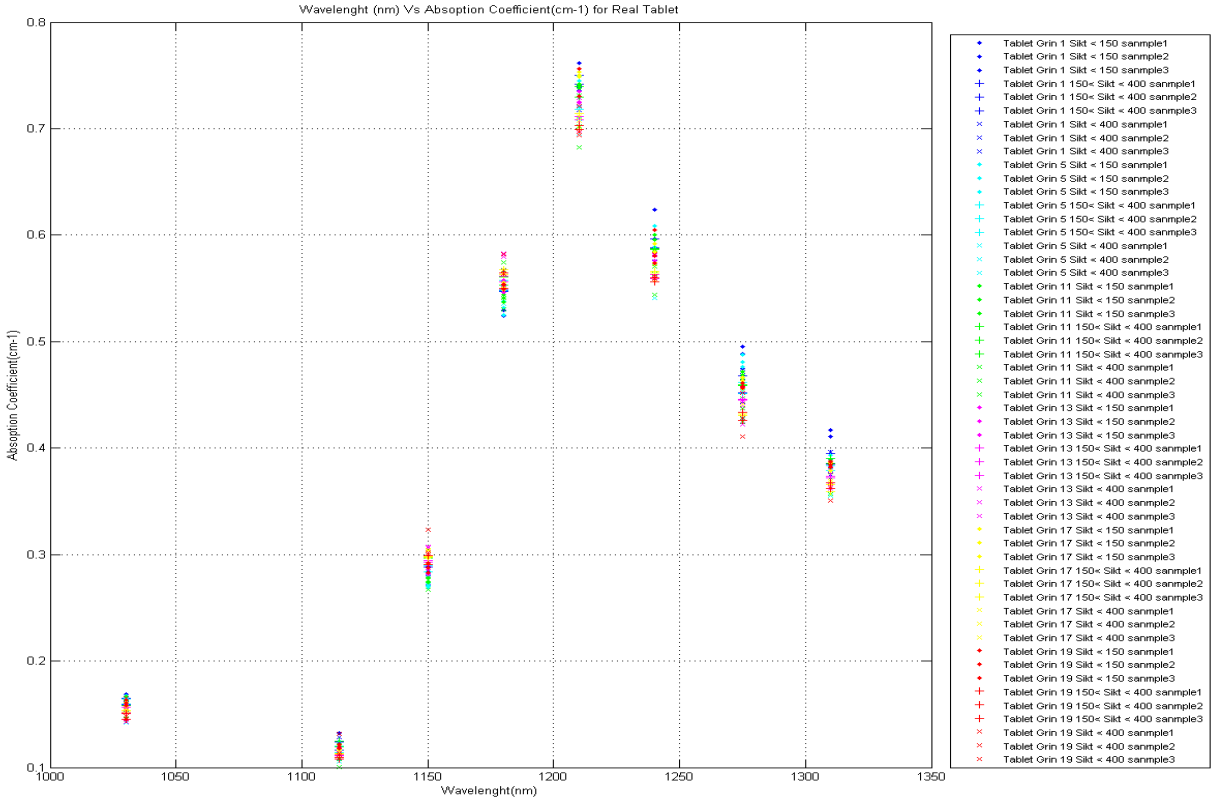

Figure8.7: Absorption coefficients (cm^{-1}) of 54 tablets at eight selective wavelengths.

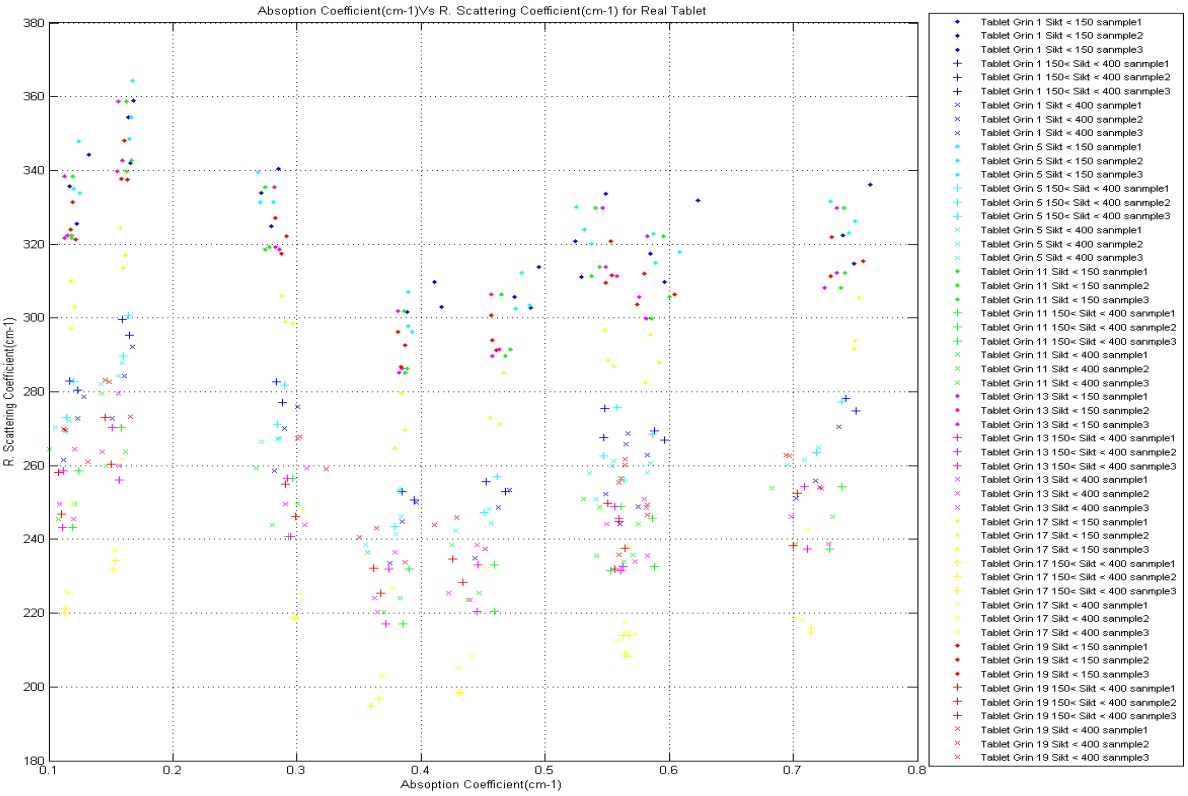

Figure8.8: Absorption coefficients (cm^{-1}) & reduced scattering coefficient (cm^{-1}) of 54 tablets at eight selective wavelengths.

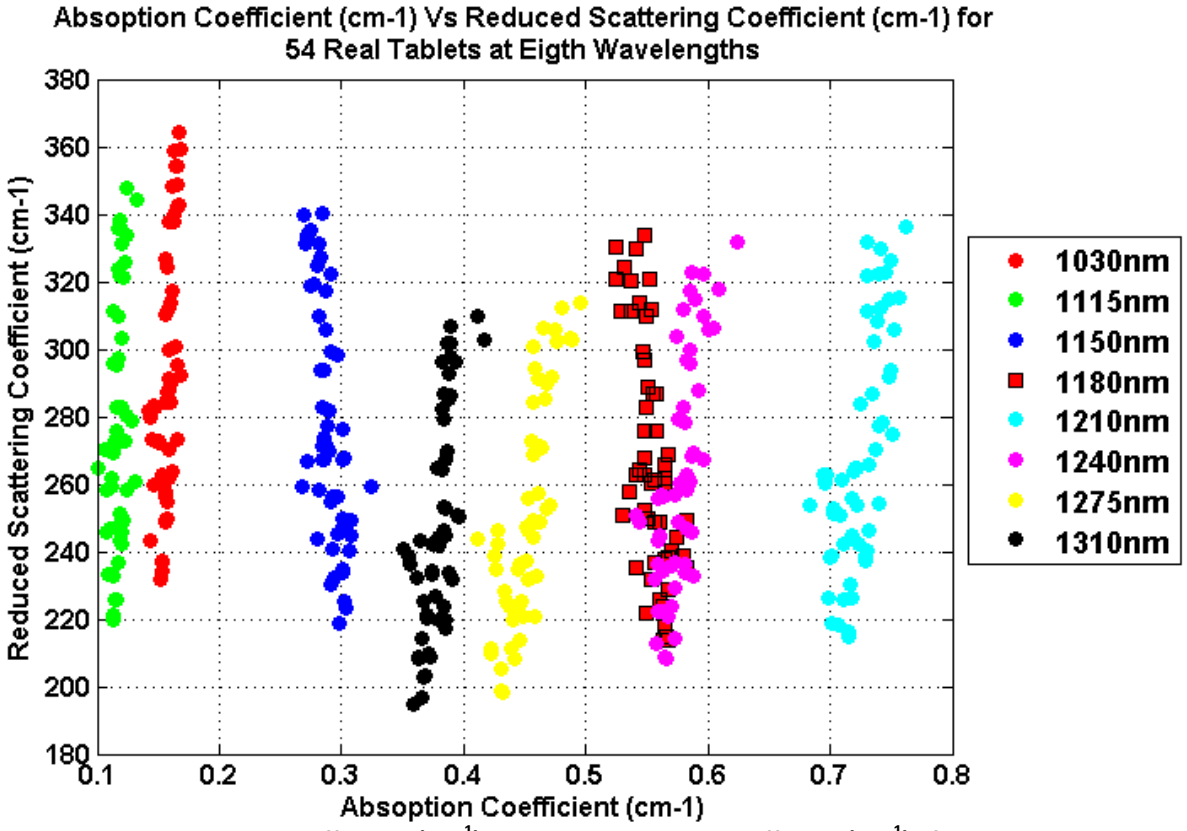

Figure8.9: Absorption coefficients (cm^{-1}) & reduced scattering coefficient (cm^{-1}) of 54 tablets at eight selective wavelengths.

After getting absorption and scattering spectra for 54 tablets separately, only absorption spectra were used in partial least square regression (PLS) regression for estimating the concentration of API in tablets. Partial least squares regression (PLS regression) is a statistical method widely used in chemo metrics and related areas.

The result is as follows:

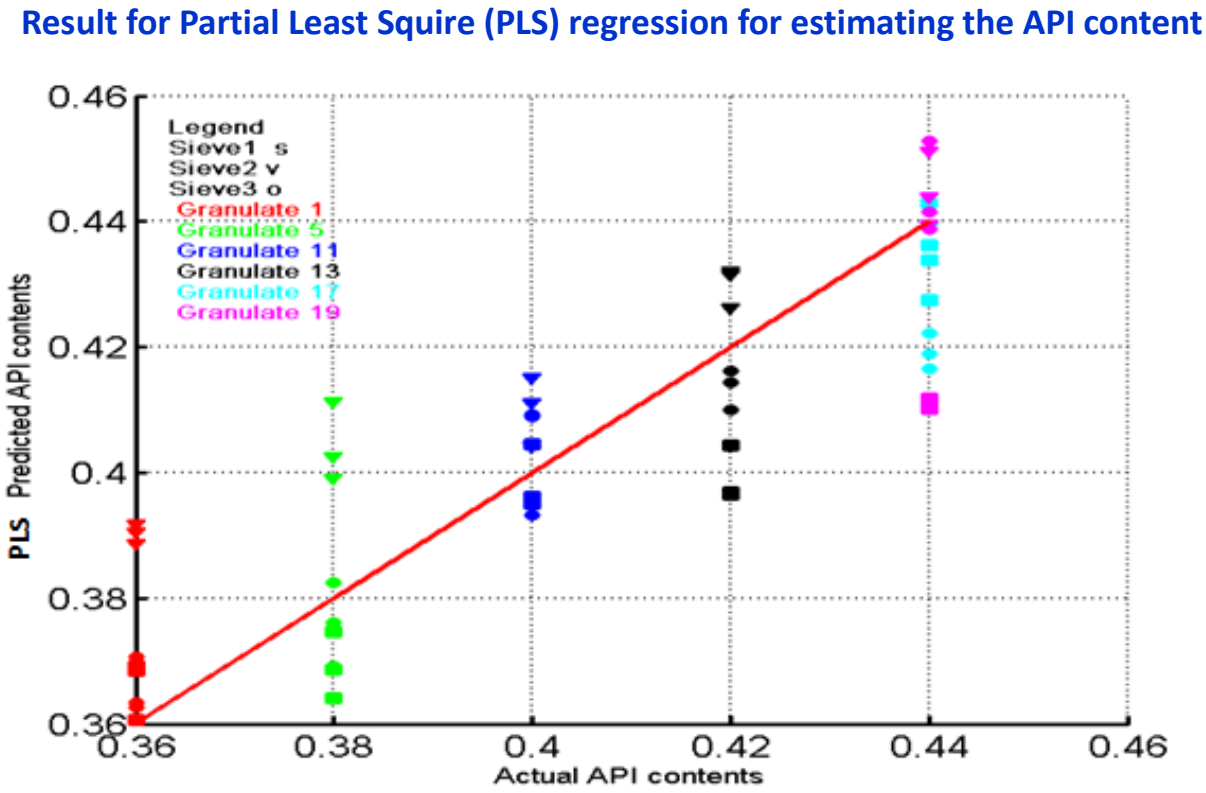

Figure8.10: Result for PLS regression for estimating the API concentration in tablet.

The API concentrations, resulted by PLS regression after evaluating optical properties by PTOFS, are within 10% of the reference value. Still we are guessing there were some problems in tablets preparation with proper contents.

Chapter 9

Conclusion:

For optimum utilization of any instrument, one the most important key parameters is to ensure the capability of the system to produce results with high accuracy and repeatability. For achieving the goal in the case of wide bandwidth Photon Time-of-Flight Spectroscopy (PTOFS), new double path optical scheme was implemented to maintain high measurement precision (uncertainty less than 1 %). The accurate calibration of the system was performed by measuring the Reduced Scattering coefficient (μ'_s) of pure Intralipid 20% and absorption coefficient (μ_a) of Indian ink solution provided by Prof. Giovanni Zaccanti, Dipartimento di Fisica, Universita' degli Studi di Firenze. New type of epoxy phantom was developed with BG36 filter crashed powder and TiO_2 for providing remarkably different absorption corresponding to different wavelength which is very effective for calibration of the system. Limited resolution effects of the system for finite source resolution and dispersion in probe pulse were also explored using this phantom. For performance assessment of the system, different types of experiment including verification of repeatability, verification of linearity for scattering and absorption, verification the fitting model have been done preparing different type of solid and liquid phantom. All these experiments showed expected results. In the case of measurement of the API of pharmaceutical tablets, spectra of 54 tablets were measured at eight wavelengths for two times. However, the results were not satisfactory. The measured concentrations are within 10% of the real concentrations. One possible reason is that there may be some problems in tablets preparation with proper contents. Besides, the accuracy of measuring API was so far hindered due to uncertainty in determination of the refractive index of the sample. Better model for evaluation of time of flight distribution can be implemented for getting more accurate optical properties. As an approach, model by Monty Carlo simulation or Partial Current Boundary can be used.

Peak Positions of Time Reference signals for sample & IRF can be different due to use different ND filters of different thickness for attenuating Time Reference Signal power. Difference in thicknesses occur difference in path lengths of time reference signal for sample & IRF and so time reference signals arrive at different time on TCSPC channel. This effect arises extra temporal drifts and affects in evaluation of correct optical properties.

Acknowledgements

I would like to thank all who encouraged me in many different ways during the courses of graduate study. Very special thanks go to Dr. Dmitry Khoptyar. I am indebted to him for providing such an interesting project and helping me entire this thesis work. Without his guidance and continuous support, this thesis would not be possible.

I am grateful to Professor Stefan Andersson-Engels for his constant encouragement and continuous guidance throughout the work.

I also want to thank Dr Muhammad Saleem, Erik Alerstam, Ahmed Soliman and all members in Biophotonics group at Atomic Physics Division for their cordial and generous help and advices.

I would like to express my gratitude to my parents and wife for their endless support for my graduate study.

Arman Ahamed Subash

Appendix:

Table6.1.2.2: Data for extrapolation of μ_a for ink series for 1st measurement at wavelengths 751nm, 833nm & 916nm.

Volume fraction of Indian Ink	751nm		833nm		916nm	
	Reduced Scattering Coefficient $\mu_s'(cm^{-1})$	Absorption Scattering Coefficient $\mu_a(cm^{-1})$	Reduced Scattering Coefficient $\mu_s'(cm^{-1})$	Absorption Scattering Coefficient $\mu_a(cm^{-1})$	Reduced Scattering Coefficient $\mu_s'(cm^{-1})$	Absorption Scattering Coefficient $\mu_a(cm^{-1})$
0.00	7.40	0.03	6.60	0.04	5.90	0.08
0.14	7.50	0.07	6.70	0.07	5.90	0.11
0.28	7.50	0.10	6.70	0.10	5.90	0.14
0.41	7.80	0.14	6.70	0.13	5.90	0.16
0.55	7.40	0.17	6.60	0.16	5.70	0.19
0.69	7.40	0.20	6.50	0.19	5.70	0.22
0.82	7.40	0.24	6.50	0.22	5.70	0.24
0.96	7.40	0.27	6.50	0.25	5.60	0.27
1.09	7.30	0.31	6.20	0.27	5.40	0.29
1.23	7.20	0.34	6.20	0.31	5.40	0.32
1.36	7.10	0.37	5.90	0.33	5.20	0.34
1.50	7.40	0.41	6.50	0.37	5.60	0.38
1.63	7.50	0.45	6.30	0.39	5.50	0.40
1.76	7.50	0.48	6.30	0.42	5.50	0.42
1.90	7.40	0.52	6.20	0.45	5.40	0.45
2.03	7.50	0.55	6.30	0.48	5.40	0.47

Table6.1.2.3: Data for extrapolation of μ_s' for Intralipid series for 1st measurement at 751nm, 833nm & 916nm.

Volume fraction of Intralipid-20	751nm		833nm		916nm	
	Absorption Scattering Coefficient $\mu_a(cm^{-1})$	Reduced Scattering Coefficient $\mu_s'(cm^{-1})$	Absorption Scattering Coefficient $\mu_a(cm^{-1})$	Reduced Scattering Coefficient $\mu_s'(cm^{-1})$	Absorption Scattering Coefficient $\mu_a(cm^{-1})$	Reduced Scattering Coefficient $\mu_s'(cm^{-1})$
0.427	0.050	1.440	0.046	1.240	0.100	1.480
0.850	0.033	2.530	0.038	2.610	0.080	2.110
1.269	0.032	3.000	0.038	2.640	0.082	2.450
1.685	0.031	3.840	0.038	3.410	0.080	3.100
2.098	0.031	4.690	0.038	4.140	0.080	3.740
2.507	0.031	5.510	0.037	4.860	0.079	4.340
2.913	0.030	6.330	0.038	5.650	0.079	5.050
3.315	0.031	7.290	0.037	6.420	0.079	5.750
3.714	0.030	8.090	0.037	7.140	0.079	6.360
4.110	0.030	8.900	0.037	7.850	0.080	7.080
4.502	0.030	9.710	0.037	8.590	0.080	7.710
4.891	0.030	10.410	0.038	9.310	0.079	8.270
5.277	0.030	11.370	0.037	10.060	0.080	9.090

Table6.1.2.4: Data for extrapolation of μ_s' for Intralipid series for 2nd measurement at 751nm, 833nm & 916nm.

Volume fraction of Intralipid-20	751nm		833nm		916nm	
	Absorption Scattering Coefficient $\mu_a(cm^{-1})$	Reduced Scattering Coefficient $\mu_s'(cm^{-1})$	Absorption Scattering Coefficient $\mu_a(cm^{-1})$	Reduced Scattering Coefficient $\mu_s'(cm^{-1})$	Absorption Scattering Coefficient $\mu_a(cm^{-1})$	Reduced Scattering Coefficient $\mu_s'(cm^{-1})$
0.420	0.031	1.200	0.041	1.180	0.082	1.180
0.836	0.033	2.240	0.035	1.990	0.077	1.900
1.249	0.031	2.930	0.036	2.550	0.076	2.290
1.658	0.030	3.810	0.036	3.380	0.077	3.060
2.064	0.030	4.700	0.037	4.150	0.077	3.690
2.466	0.030	5.760	0.035	5.130	0.075	4.690
2.865	0.029	6.380	0.036	5.680	0.076	5.000
3.261	0.030	7.030	0.036	6.170	0.078	5.470
3.654	0.030	7.870	0.036	6.970	0.078	6.230
4.044	0.029	8.590	0.036	7.660	0.078	6.830
4.430	0.030	9.390	0.036	8.280	0.078	7.440
4.814	0.030	10.140	0.036	9.030	0.079	8.090
5.194	0.030	10.960	0.036	9.640	0.078	8.610
5.571	0.029	11.670	0.036	10.290	0.080	9.360

6.2.3: Optical Properties of Phantoms for Absorption Series and Verifying Linearity of the System:

Wavelength In nm	Tablet with ink 0%		Tablet with ink 0.0165%		Tablet with ink 0.036%		Tablet with ink 0.0508%		Tablet with ink 0.0667%	
	Absorption Scattering Coefficient $\mu_a(cm^{-1})$	Reduced Scattering Coefficient $\mu_s'(cm^{-1})$	Absorption Scattering Coefficient $\mu_a(cm^{-1})$	Reduced Scattering Coefficient $\mu_s'(cm^{-1})$	Absorption Scattering Coefficient $\mu_a(cm^{-1})$	Reduced Scattering Coefficient $\mu_s'(cm^{-1})$	Absorption Scattering Coefficient $\mu_a(cm^{-1})$	Reduced Scattering Coefficient $\mu_s'(cm^{-1})$	Absorption Scattering Coefficient $\mu_a(cm^{-1})$	Reduced Scattering Coefficient $\mu_s'(cm^{-1})$
1100	0.09	121.29	0.48	123.34	1.07	122.98	1.50	124.18	1.78	121.37
1148	0.42	119.70	0.81	122.18	1.41	123.07	1.85	124.24	2.13	121.82
1158	0.42	116.15	0.80	118.72	1.38	118.42	1.80	119.29	2.06	117.40
1190	0.63	118.48	1.03	121.22	1.59	119.63	1.96	120.52	2.27	118.48
1206	0.53	117.89	0.90	118.40	1.51	120.82	1.87	118.35	2.17	118.50
1226	0.46	116.83	0.82	117.79	1.40	118.11	1.79	117.69	2.08	118.01
1246	0.34	114.62	0.70	116.99	1.28	117.25	1.61	114.72	1.95	116.05
1270	0.22	110.04	0.57	110.92	1.13	111.43	1.51	110.33	1.78	110.24
1298	0.17	110.07	0.53	111.77	1.06	111.33	1.44	110.81	1.70	109.70
1322	0.18	107.22	0.53	109.74	1.09	110.92	1.45	109.28	1.71	109.78

6.2.4 Optical Properties of Phantoms for Absorption Series and Verifying Linearity of the System:

Wavelength In nm	Tablet with TiO_2 7.54%		Tablet with TiO_2 14.1%		Tablet with TiO_2 19.7%		Tablet with TiO_2 24.6%		Tablet with TiO_2 29%	
	Absorption Scattering Coefficient $\mu_a(cm^{-1})$	Reduced Scattering Coefficient $\mu_s'(cm^{-1})$	Absorption Scattering Coefficient $\mu_a(cm^{-1})$	Reduced Scattering Coefficient $\mu_s'(cm^{-1})$	Absorption Scattering Coefficient $\mu_a(cm^{-1})$	Reduced Scattering Coefficient $\mu_s'(cm^{-1})$	Absorption Scattering Coefficient $\mu_a(cm^{-1})$	Reduced Scattering Coefficient $\mu_s'(cm^{-1})$	Absorption Scattering Coefficient $\mu_a(cm^{-1})$	Reduced Scattering Coefficient $\mu_s'(cm^{-1})$
1100	0.09	108.82	0.06	205.02	0.05	286.90	0.05	359.97	0.05	436.75
1148	0.46	104.27	0.41	199.32	0.38	275.06	0.36	343.62	0.34	414.95
1158	0.41	105.23	0.37	198.61	0.34	275.08	0.32	344.61	0.32	421.24
1190	0.76	105.42	0.67	196.10	0.61	267.76	0.59	338.65	0.56	406.07
1206	0.55	103.32	0.50	193.87	0.47	269.69	0.46	340.76	0.42	403.74
1226	0.51	103.35	0.46	194.42	0.42	268.11	0.40	337.49	0.38	406.93
1246	0.37	102.31	0.33	191.87	0.30	265.05	0.29	334.35	0.28	400.96
1270	0.26	99.58	0.22	187.73	0.21	262.04	0.20	328.42	0.19	395.94
1298	0.19	100.11	0.16	187.96	0.14	259.78	0.14	327.04	0.14	394.42
1322	0.20	99.81	0.17	185.83	0.16	259.12	0.15	321.78	0.15	389.04

Table 6.3 Optical Properties of Phantoms for verification the Stability of the System

Wavelength In nm	2.02mm tablet		2.49mm tablet		2.885mm tablet		3.43mm tablet		3.76mm tablet	
	Absorption Scattering Coefficient $\mu_a(cm^{-1})$	Reduced Scattering Coefficient $\mu_s'(cm^{-1})$	Absorption Scattering Coefficient $\mu_a(cm^{-1})$	Reduced Scattering Coefficient $\mu_s'(cm^{-1})$	Absorption Scattering Coefficient $\mu_a(cm^{-1})$	Reduced Scattering Coefficient $\mu_s'(cm^{-1})$	Absorption Scattering Coefficient $\mu_a(cm^{-1})$	Reduced Scattering Coefficient $\mu_s'(cm^{-1})$	Absorption Scattering Coefficient $\mu_a(cm^{-1})$	Reduced Scattering Coefficient $\mu_s'(cm^{-1})$
1100	0.06	164.42	0.05	162.23	0.06	163.96	0.06	163.52	0.06	163.04
1148	0.39	150.21	0.40	151.33	0.42	152.75	0.42	153.50	0.42	152.43
1158	0.36	152.96	0.35	150.53	0.36	151.27	0.36	149.66	0.37	150.89
1190	0.73	149.46	0.72	147.18	0.72	146.72	0.71	145.00	0.71	144.63
1206	0.53	145.40	0.55	145.54	0.54	145.54	0.55	144.27	0.54	142.92
1226	0.48	143.18	0.49	141.85	0.49	140.62	0.49	139.54	0.50	140.40
1246	0.35	135.74	0.36	135.80	0.36	134.74	0.36	135.16	0.36	135.45
1270	0.24	131.02	0.23	130.04	0.24	130.52	0.24	129.34	0.24	130.10
1298	0.16	126.52	0.16	126.70	0.17	126.96	0.17	126.05	0.17	125.83
1322	0.17	124.24	0.17	123.98	0.17	123.43	0.17	122.93	0.17	122.11

6.3 Optical Properties of Phantoms for verification of the Results with Different Fit Ranges:

Fitting range, % of the PTOF maximum	Phantom with high absorption at 786nm		Phantom with low absorption at 830nm	
	Absorption Coefficient $\mu_a(cm^{-1})$	Reduced Scattering Coefficient $\mu_s'(cm^{-1})$	Absorption Coefficient $\mu_a(cm^{-1})$	Reduced Scattering Coefficient $\mu_s'(cm^{-1})$
10	0.31	3.88	0.04	5.95
20	0.31	3.90	0.04	5.95
30	0.31	3.92	0.04	5.96
40	0.31	3.92	0.04	5.97
50	0.32	3.94	0.04	5.97
60	0.32	3.94	0.04	5.97
70	0.32	4.00	0.04	5.97
80	0.32	4.06	0.04	5.97

6.4 Pharmaceuticals tablets Description:

Primary ID	granules	API	API Conc.	sieve frac	Particle size	tablet	tablet	weight	height	diameter
		(mg)	(mg/g)					(mg)	(mm)	(mm)
1-1-1	1	180	286.2	1	<150µm	1	T1	518.2	3.02	13
1-2-1	1	180	286.2	2	150-400µum	1	T1	499.5	2.88	13
1-3-1	1	180	286.2	3	>400µm	1	T1	494.7	2.87	13
5-1-1	5	190	302.1	1	<150µm	1	T1	498.1	2.88	13
5-2-1	5	190	302.1	2	150-400µum	1	T1	497.5	2.87	13
5-3-1	5	190	302.1	3	>400µm	1	T1	496.5	2.92	13
11-1-1	11	200	318.0	1	<150µm	1	T1	488.9	2.83	13
11-2-1	11	200	318.0	2	150-400µum	1	T1	495.1	2.85	13
11-3-1	11	200	318.0	3	>400µm	1	T1	502.5	2.92	13
13-1-1	13	210	333.9	1	<150µm	1	T1	485.3	2.82	13
13-2-1	13	210	333.9	2	150-400µum	1	T1	514.1	2.97	13
13-3-1	13	210	333.9	3	>400µm	1	T1	499.3	2.93	N/A
17-1-1	17	220	349.8	1	<150µm	1	T1	497.5	2.91	13
17-2-1	17	220	349.8	2	150-400µum	1	T1	499.3	2.90	13
17-3-1	17	220	349.8	3	>400µm	1	T1	501.6	2.93	13
19-1-d	19	220	349.8	1	<150µm	d	T1	483.8	2.83	13
19-2-1	19	220	349.8	2	150-400µum	1	T1	469.8	2.73	13
19-3-D	19	220	349.8	3	>400µm	D	T1	496.6	2.98	13

Reference:

1. Tomas Svensson. ‘’Pharmaceutical and Biomedical Applications of Spectroscopy in the Photon Migration Regime’’. PhD thesis, Division of Atomic Physics Department of Physics, Faculty of Engineering, LTH, Lund University, 2008. P.19-22.
2. Daniele Contini, Fabrizio Martelli, and Giovanni Zaccanti “Photon migration through a turbid slab described by a model based on diffusion approximation. I. Theory.” APPLIED OPTICS y Vol. 36, No. 19 y 1 July 1997.
3. R. C. Haskell, L. O. Svaasand, T. T. Tsay, T. C. Feng, M. S. McAdams, and B. J. Tromberg, “Boundary conditions for the diffusion equation in radiative transfer,” J. Opt. Soc. Am. A **11,** 2727–2741 ~1994.
4. A. Ishimaru, Wave Propagation and Scattering in Random Media ~Academic, New York, 1978, Chap. 7, p. 157; Chap. 9, p. 175.
5. S. Chandrasekhar, Radiative Transfer ~Oxford, New York, 1969, Chap. 1, p. 9.
6. M. S. Patterson, S. J. Madsen, J. D. Moulton, and B. C. Wilson, “Diffusion equation representation of photon migration in tissue,” in IEEE Microwave Theory and Techniques Symposium Digest ~IEEE, New York, 1991!, Vol. BB-1, pp. 905–908.
7. Yu Chen’’ CONTRAST ENHANCEMENT FOR DIFFUSE OPTICAL SPECTROSCOPY AND IMAGING: PHASE CANCELLATION AND TARGETED FLUORESCENCE IN CANCER DETECTION ‘’.A Dissertation in Bioengineering, University of Pennsylvania 2003.
8. H. S. Carslaw and J. C. Jaeger, Conduction of Heat in Solids (Oxford, London, 1959).

9. Erik Alerstam, Stefan Andersson-Engels, and Tomas Svensson, "Improved accuracy in time-resolved diffuse reflectance spectroscopy," Opt. Express **16**, 10440-10454 (2008).
10. Fianium Ltd. Manual for femto power 1060, tunable super continuum source, sc450-AOTF.
11. Rüdiger Paschotta. http://www.rp-photonics.com/supercontinuum(underscore) generation. html. Encyclopedia of Laser Physics and Technology, 9 March 2009. 10 March 2009.
12. Near Infrared Spectroscopy for measuring Optical Parameters in Flour and Grain-Viveka Anderberg-Master's thesis Lund University Faculty of Engineering, LTH June 2009.
13. Jesper Hakansson and Shazia Farooq ‘’Time of Flight Absorption and Scattering spectroscopy of Pharmaceutical Tablets’’. Atomic Physics Division, Lund University. December 2010.P:12.
14. Tomas Svensson ‘’Pharmaceutical and Biomedical Applications of Spectroscopy in the Photon Migration Regime’’ Doctoral Thesis 2008, chapter 3, page-39.

15. JCGM 200:2008 International vocabulary of metrology — Basic and general concepts and associated terms (VIM)

16. http://en.wikipedia.org/wiki/Accuracy_and_precision

17. D. Khoptyar, M. Saleem, A.A. Subash, S. Andersson-Engels, “Wide Bandwidth Time of Flight Spectroscopy of Turbid Media” **III International Symposium on TOPICAL PROBLEMS OF BIOPHOTONICS – 2011**, St.-Petersburg- Nizhny Novgorod, Russia, 16-22 July 2011.

18. Bruce Moision and William Farr ‘’Communication Limits Due to Photon Detector Jitter’’. IEEE PHOTONICS TECHNOLOGY LETTERS, VOL. 20, NO. 9, MAY 1, 2008
19. L. Spinelli, A. Pifferi, A. Torricelli, R. Cubeddu, P. Di Ninni, F. Martelli, G. Zaccanti, F. Foschum, A. Kienle, M. Mazurenka, H. Wabnitz, M. Kacprzak, N. Zolek, D. Milej, and A. Liebert, "Towards the Definition of Accurately Calibrated Liquid Phantoms for Photon Migration at NIR Wavelengths: A Multi-Laboratory Study," in *Biomedical Optics*, OSA Technical Digest (CD) (Optical Society of America, 2010), paper BTuD47.
20. S. J. Madsen, M. S. Patterson, and B. C. Wilson, “The use of india ink as an optical absorber in tissue-simulating phantoms,” *Phys. Med. Biol.* **37**_4_, 985–993 _1992_.

21. H. J. van Staveren, C. J. M. Moes, J. van Marle, S. A. Prahl, and M.J. C. Vangemert, “Light scattering in intralipid-10-percent in the wavelength range of 400–1100 nm,” *Appl. Opt.* **30**_31_, 4507–4514 _1991_.

22. S. T. Flock, S. L. Jacques, B. C. Wilson, W. M. Star, and M. J. C. Vangemert, “Optical properties of intralipida phantom medium for light-propagation studies,” *Lasers Surg. Med.* **12**_5_, 510–519 _1992_.
23. E. Alerstam, S. Andersson-Engels, T. Svensson, “White Monte Carlo for time-resolved photon migration”, J. Biomed. Optics 13 041304 (2008).
24. Wikipedia. http://en.wikipedia.org/wiki/Student%27s_t-distribution
25. Schott Data Sheet for BG36 filter.

The End

Comments:

In this diploma project, one of the aims was to precisely determine the drug concentration (API) of pharmaceutical tablets using photon time of flight spectroscopy (PTOFS) and multivariate analysis. For achieving this goal, in the pilot experiment 54 tablets were prepared from Astra Zeneca (by one of former thesis students) which have six different concentrations of drug (granulates) three different levels of scattering (sieve size). Then, absorption and reduced scattering coefficients were evaluated implementing photon time of flight spectroscopy and partial least square (PLS) regression analysis was made with absorption coefficient values in order to estimate the drug concentration precisely. During the thesis work, the acquired results from regression analysis were within 10% of the reference values and incompetence of preparing the tablets with correct design concentrations was assumed as one of probable reasons for this unsatisfactory result. As a consequence, 18 tablets of six different drug concentrations with three different levels of scattering were sent to Astra Zeneca in order to evaluate and check their drug concentration using reference analysis method. The outcome of the investigation showed completely different drug concentrations in tablets from the design concentrations and these are as follows:

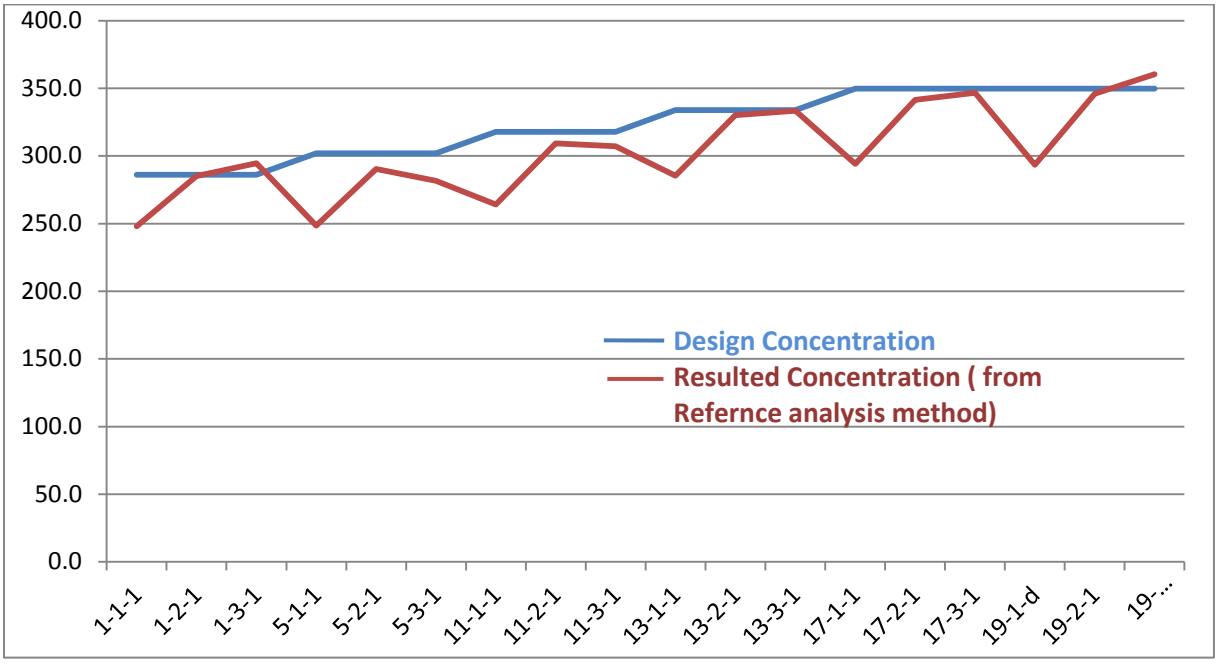

Figure1: Comparison of Design concentration and resulted concentration from reference analysis.

This is the new result from Partial Least Square (PLS) regression.

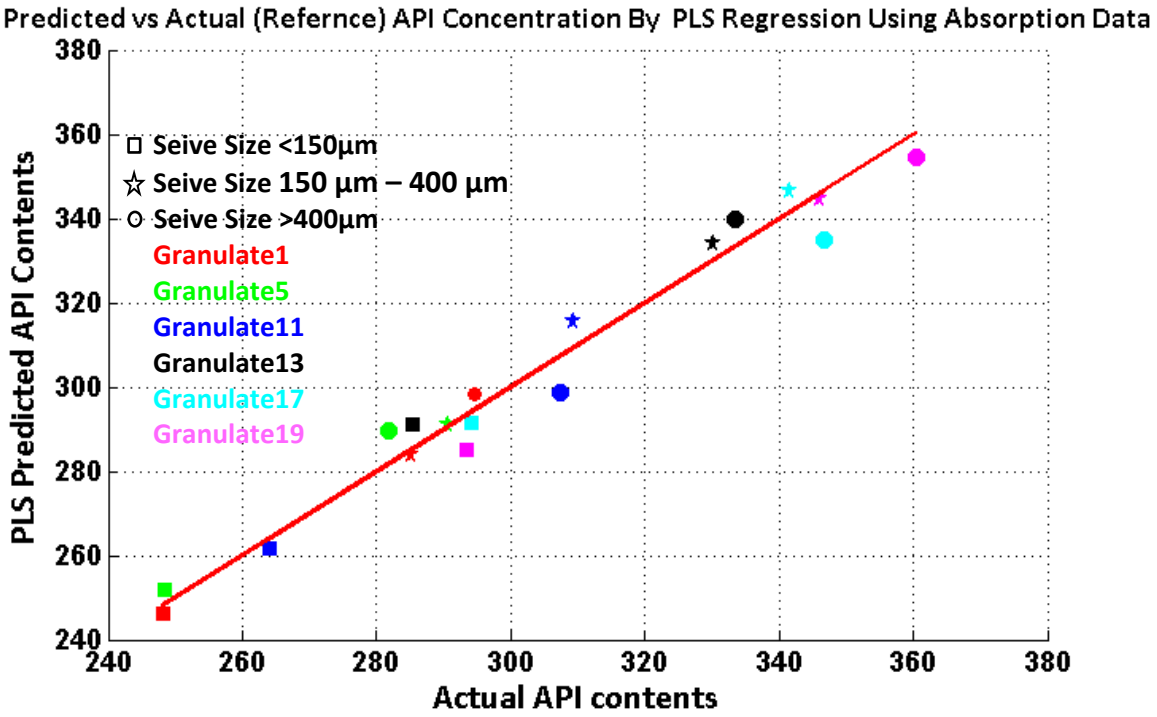

Figure2: Result for PLS regression for estimating the API concentration in tablet.

According to new result, the Predicted API concentrations by PLS regression analysis are quite comparable with the new drug concentrations obtained from reference analysis.